Benefits of GPS-Aided Altitude Estimation in Multi Rotor Drones

by

Vincent van der Merwe

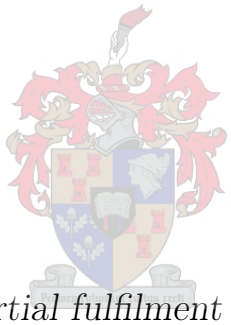

Thesis presented in partial fulfilment of the requirements for the degree of Master of Engineering (Mechatronic) in the Faculty of Engineering at Stellenbosch University

Supervisor: Dr. WJ. Smit

March 2021

Declaration

By submitting this thesis electronically, I declare that the entirety of the work contained therein is my own, original work, that I am the sole author thereof (save to the extent explicitly otherwise stated), that reproduction and publication thereof by Stellenbosch University will not infringe any third party rights and that I have not previously in its entirety or in part submitted it for obtaining any qualification.

Date: 20/11/2020 .....

Abstract

Benefits of GPS-Aided Altitude Estimation in Multi Rotor Drones

V. van der Merwe

Department of Mechanical and Mechatronic Engineering,
University of Stellenbosch,
Private Bag X1, Matieland 7602, South Africa.

Thesis: MEng (Mech)

April 2021

Ongoing research investigates the use of drones for heliostat calibration, however, is limited by the quality of the collected data and thus the positional accuracy of the drone. Evaluation of various drone models identified the altitude to be the least accurate and in most cases was measured using a single barometer, which is prone to sensor drift and disturbances.

To address the issue, the study proposed GPS-aided altitude estimation using a Kalman filter, in addition to sensor fusion based on Covariance Intersection with the testing done via simulations. In addition to testing a GPS and RTK-GPS, the estimation and correction of the barometer drift were evaluated. Lastly, the relationship between the altitude and drift estimation accuracy based on differences in the sensor noise ratios were also investigated.

The results indicated minimal benefit and effectiveness in the RTK-GPS and GPS cases, thus exhibiting single sensor dominance. The sensor noise ratios illustrate the benefits of GPS-aided altitude estimation, with the improvement in accuracy being largely dependent on the difference in the ratio. Furthermore, a window for optimal benefit was identified between the ratios of 0.6 and 4, with the improvement in accuracy rapidly decreasing as the ratio becomes less than unity.

The research provides insight regarding the expected accuracy improvement of the altitude estimate for a wide range of sensor ratios, while also illustrating the accuracy and benefits of drift estimation and correction when using GPS altitude measurements and sensor fusion.

Uittreksel

Voordele van GPS-Gesteunde Hoogte Afskatting in Multi-Rotor Hommeltuie

("Benefits of GPS-Aided Altitude Estimation in Multi Rotor Drones")

V. van der Merwe

Departement Meganiese en Megatroniese Ingenieurswese,
Universiteit van Stellenbosch,
Privaatsak X1, Matieland 7602, Suid Afrika.

Tesis: MIng (Meg)

April 2021

Voortgesette navorsing ondersoek die gebruik van hommeltuie vir heliostaatkalibrasie, maar word beperk deur die kwaliteit van die versamelde data en dus die posisionele akkuraatheid van die hommeltuig. Die evaluering van verskillende hommeltuigmodelle het aangedui dat die hoogte die minste akkuraat is en in meeste gevalle deur 'n enkele barometer gemeet word, wat geneig is tot sensordryf en versteurings. Om die probleem aan te spreek, het die studie GPS-gesteunde hoogte afskatting voorgestel deur middel van 'n Kalman-filter, asook sensorfusie gebaseer op kovariansie-kruising, en die toetse uitgevoer deur simulasies. Insluitend die toets van 'n GPS en 'n RTK-GPS, is die afskatting en regstelling van die barometerdryf geevalueer. Laastens is die verband tussen die akkuraatheid van die hoogte- en drywingsafskattings gebaseer op verskille in die sensor geraas verhoudings ook ondersoek.

Die resultate het 'n minimale voordeel en effektiwiteit getoon in die RTK-GPS en GPS-gevalle en toon die oorheersing van enkele sensors. Die sensor geraas verhoudings illustreer die voordele van GPS-ondersteunde hoogte afskatting, met die verbetering van die akkuraatheid, wat grootliks afhang van die verskil in die geraas verhouding. Verder is 'n interval vir optimale voordeel geïdentifiseer tussen die verhoudings van 0.6 en 4, met die verbetering in akkuraatheid wat vinnig afneem namate die verhouding verlaag word vanaf eenheid. Die navorsing bied insig ten opsigte van die verwagte akkuraatheidsverbetering van die hoogteafskatting vir 'n wye verskeidenheid sensor verhoudings, terwyl dit ook die akkuraatheid en voordele van drywingsafskatting en -korreksie illustreer tydens die gebruik van GPS-hoogtemetings en sensorfusie.

Acknowledgements

I wish to express my sincere gratitude to the following people:

To my supervisor, Dr Willie Smit, for his unparalleled guidance, patience, and enthusiasm. For his inspirational willingness to help and keen insight. It has truly been an honour and privilege to study under his supervision

To my family for their unwavering emotional and financial support. For their love, patience, and sacrifice. And most importantly, for affording me the privilege and opportunity to pursue an education.

Contents

List of Figures

List of Tables

Nomenclature

Constants

M	28.964×10^{-3}	[kg/mol]
R	8.314	[J/mol·K]
g	9.81	[m/s^2]

Variables

θ	Pitch	[rad]
ϕ	Roll	[rad]
ψ	Yaw	[rad]
μ	Mean	[m]
σ	Standard Deviation	[m]
σ^2	Variance	[m^2]
Δt	Sample Time	[s]
z	Vertical Position (Altitude)	[m]
$\dot{z}$	Vertical Velocity	[m/s]
$\ddot{z}$	Vertical Acceleration	[m/s^2]

Vectors and Tensors

B	Control Input Matrix
C	CI Fusion Weight Vector
F	State Transition Matrix
H	Observation Matrix
I	Identity Matrix
K	Optimal Kalman Gain Matrix
P	Estimate Covariance Matrix
Q	Process Noise Matrix

R	Measurement Noise Covariance Matrix
u	Control Input Vector
x	State Estimate Vector
y	Measurement Residual Vector
z	Sensor Measurement Vector

Subscripts

k	Current Timestep
$k-1$	Previous Timestep
1	Kalman Barometer Altitude State
2	Kalman GPS Altitude State
3	Kalman RTK-GPS Altitude State
4	Kalman Vertical Velocity State
5	Kalman Barometer Drift State

Superscripts

$\wedge$	Estimate
-1	Inverse
$-$	Predicted
T	Transpose
$+$	Updated

Abbreviations

CI	Covariance Intersection
CPU	Central Processing Unit
CSP	Concentrated Solar Power
CVM	Constant Velocity Model
FDE	Fault Detection and Exclusion
GMF	Generalised Millmans Formula
GNSS	Global Navigation Satellite System
GPS	Global Positioning System
IBI	Integrated Baro Inertial
IBIG	Integrated Baro Inertial GPS
IGS	International Geosynthetics Society
IIG	Integrated Inertial GPS
IMU	Inertial Measurement Unit
INS	Inertial Navigation System

MLE	Maximum Likelihood Estimation
NGA	National Geospatial-Intelligence Agency
OKF	Optimal Kalman Filter
RAIM	Receiver Autonomous Integrity Monitoring
RKF	Robust Kalman Filter
RMSE	Root Mean Squared Error
RTK	Real-Time Kinematic
STERG	Solar Thermal Energy Research Group
VTOL	Vertical Take-Off and Landing

Chapter 1

Introduction

1.1 Background

This research project falls under the Solar Thermal Energy Research Group (STERG) at Stellenbosch University. STERG mostly investigates various methods of solar thermal energy generation and storage. In the case of energy generation, much of the ongoing research is in Concentrated Solar Power (CSP), more specifically the Power Tower configuration where heliostats focus the solar rays onto a central tower-mounted receiver. Figure 1.1 illustrates one such CSP Plant, namely, Torresol's Gemasolar in Spain.

Figure 1.1: Gemasolar CSP (Torresol, 2017)

Some of the research projects investigate the use of robots or drones to automate the tasks required in such fields, such as the washing and calibration of heliostats. The use of drones for the calibration procedure has shown promise, in which drones are used to gather data regarding the orientation of heliostats. The gathered data is then used to calibrate the relevant heliostats. However, the quality of the collected data depends on how well the drone knows its physical position. This can be referred to the positional accuracy of the drone, which describes where the drone estimates it is in relation to where it actually is. Improving the positional accuracy of the drone would improve the quality of the data gathered and thus yield a better calibration of the heliostats.

1.2 Specific Dilemma

The position of a drone is normally described using six degrees of freedom. This being the translation in three perpendicular axes along with rotation about the three axes. Initial investigation on the reported positional accuracy of commercially available drones revealed the positioning in the vertical axis is the least accurate. Some confirmation was obtained by observing the altitude of drones during flight. In most cases, when given a position hold command, variations in altitude were more noticeable in comparison to those of the lateral and longitudinal directions.

Lastly, reviewing literature on the accuracy of Geo-surveying using drones also indicated the vertical axis as the least accurate, with the RMSE of the drone's vertical accuracy being 1.5 (Buczkowski, 2017) to 2.8 (DroneDeploy, 2020) times that of its horizontal accuracy. Consequently, it is necessary to address the accuracy of the reported altitude.

1.3 Status of the Problem

Following the concept of drone-based heliostat calibration, the positional accuracy of the drone requires improvement to allow for higher quality data and thus better calibration. More specifically, the accuracy of the altitude estimate is to be addressed as it is the least accurate.

Initial investigation of various commercially available drones and the PX4 flight stack revealed the variety of sensors used in altitude estimation. The PX4 flight stack was used as the focus for this study as it is open-source, widely used in academia, and supported by the Pixhawk series flight controllers. The variety of different altitude sensors typically implemented, but not limited to, comprises of the following:

- Barometer
- Ultrasonic Range Finder

- GPS

Barometers are the most common and, in most cases, the only sensor used for altitude estimation. This is done by measuring the air pressure at altitude which is used and compared to the measured air pressure at take-off (Ground level). The pressure difference is used in the barometric formula to determine the difference in height, therefore altitude. While being accurate and having a fast sample time, barometers are prone to drift, where over extended periods of time the accuracy of the readings deteriorate at an unknown rate and become unreliable.

Ultrasonic range finders are sometimes used to measure height above ground level; however, they have a very limited range. Objects on the ground like heliostats would lead to incorrect height measurements. Hence, the use of ultrasonic sensors is typically used for landing and obstacle avoidance.

The Global Navigation Satellite System (GNSS) is a collection of satellites used for geolocation and timing solutions. The Global Positioning System (GPS) forms part of the GNSS, and the term has become synonymous when referring to geolocation. GPS sensors are very rarely used for altitude estimation. This is mainly due to its very high inaccuracy in comparison to other sensors such as a barometer. GPS's also suffer from errors and perturbations when the signals pass through the ionosphere and troposphere, with the former being more significant. As mentioned, an elevation measurement is also provided, however, this is roughly two to three times less accurate than that of the lateral and longitudinal measurements as can be seen in Table 1.1.

Table 1.1: Daily Average GPS Position Errors for 2019 (Renfro *et al.*, 2019)

Sensor	**Horizontal** (m)	**Vertical** (m)
Median	1.25	2.12
Mean	2.10	3.76
Standard Deviation	3.60	6.71
Maximum	33.63	72.95

The large variation in the magnitude of the horizontal and vertical errors is mostly due to the positioning of the satellites relative to the receiver during trilateration. Most of the satellites would be close to the horizon, whereas, for more accurate altitude measurements, the satellites would need to be almost directly above the receiver.

1.4 Possible Solution

From the previous section, the need to address the accuracy of the altitude has been motivated and a variety of suitable sensors were identified. As the drone would be flying over the heliostat field, the altitude readings from an ultrasonic sensor would vary constantly as the heliostats would act as obstructions. This would result in sudden large changes in altitude should the drone fly over a heliostat. Consequently, the ultrasonic range finder is eliminated due to limitations and specific use cases. Thus, the barometer and GPS remain, which would be the two main sensors implemented in the proposed solution.

The proposed solution would be to implement a GPS-aided altitude estimation algorithm. This would involve using both the barometer and GPS in an attempt to compliment the sensors, remove shortcomings, and potentially increase accuracy. Furthermore, the unknown barometer drift is to be addressed to eliminate or minimize its effect and improve the long term accuracy of the barometer. To address the barometer drift, it is to be estimated as a state using a Kalman filter, similar to the altitude estimates for each of the implemented sensors.

To use both sensors effectively, sensor fusion needs to be implemented as well to combine the two altitude estimates of the sensors. Additionally, a different type of GPS is also to be tested, namely, a Real-Time Kinematic (RTK) system which is far more accurate than a normal GPS as well as a barometer. As standard GPS is significantly less accurate than a barometer and an RTK-GPS is significantly more accurate, a broad range is created where the barometer is near the centre in terms of accuracy.

The proposed solution is to be tested using simulations, as it would allow for a controlled environment in which different setups can be tested under identical conditions and prevent inaccuracies caused by external factors.

Lastly, using simulations, different GPS or RTK sensors are to be modelled and implemented over the mentioned range. The modelled sensors are to be tested to illustrate and identify the improvement in positional accuracy in terms of the various sensor noise ratios.

1.5 Aim and Objectives

This research aims to identify and illustrate the benefits of GPS-aided altitude estimation.

In summary, the main objectives are:

- set up a simulation environment capable of accurately reflecting the real-world characteristics of quadcopter flight.
- identify, model, and simulate the sensors to be used and evaluated.
- formulate, derive, and implement a method for sensor fusion.
- evaluate and assess the various implemented sensor combinations.
- determine and illustrate a relationship for the optimal sensor combination.

Chapter 2

Literature Review

This chapter covers a review of existing literature and sources applicable to the altitude estimation of drones. It acts as additional information regarding the implementation and benefits of various altitude estimation methods and the various sensors used.

Firstly, brief overviews of barometric altitude measurement and estimation are given, as well as the improvement in the accuracy of GPS-based altitude measurements. This is followed by a section regarding a variety of studies pertaining to the combination of barometric and GPS altitude for the case of altitude estimation. In addition, some notable mentions regarding sensor fusion and combination are also included. These act as potential methods of fusion but are excluded from the previous section as they do not feature barometric and GPS altitude fusion. Lastly, the various sources of literature are interpreted, assessed, and compared, followed by a summary of the key findings and issues.

2.1 Barometric Altitude Measurement

This section covers the use of barometric pressure sensors for the measurement of altitude or vertical displacement.

An investigation of barometric altitude measurements was done by Ho *et al.* (2018), using four different smartphones under various conditions. The authors investigated the effects of temperature changes in controlled and uncontrolled environments as well as the effect of changes in air pressure.

The study found that the various barometric sensors were resistant to an increase in temperature, thus maintaining accuracy. Furthermore, sudden changes in air pressure caused by passing vehicles resulted in altitude variations of 1.48 to 1.74 m for the tested sensors. Thus, illustrating and confirming the susceptibility of barometers to external disturbances, which is a common problem present in the control of quadcopters when used for altitude estima-

tion.

Zhang *et al.* (2019) studied altitude estimation in the form of a Kalman filter using a barometer and Inertial Measurement Unit (IMU) readings. This comprised of integration of the vertical acceleration to obtain the vertical position and velocity which was compared to a velocity and position measured using the barometer. The difference or residual is used in a Kalman filter to provide an estimate which is added to the IMU altitude and velocity as the optimal estimate.

The study only shows a small window of 30 seconds for the altitude estimate, thus the effect of barometer drift is not visible as it would be negligible. The authors' work illustrates the use of barometers to correct the growing integration errors present in INS solutions, albeit being over a small time span, and thus warrants additional study regarding the growing barometer drift and its effect.

Altitude fusion of an Inertial Navigation System (INS) and barometer was also investigated by Wei *et al.* (2016) using a complementary filter and differential measurements. Differential measurements of the barometric altitude are implemented using two barometers, with one acting as a base station and the other as a rover. In addition to temperature compensation, the difference between the sensors is computed and fused with the IMU acceleration using a complementary filter to provide an altitude measurement. In conclusion, the proposed method is effective in removing the barometer drift, however, the final solution exhibits noticeable levels of stochastic noise.

2.2 Improvement in the Accuracy of GPS Altitude Measurements

This section acts as an insight into the improvement in GPS altitude measurements and the increase of its applicability for altitude estimation.

Tables 2.1 and 2.2 summarize the yearly mean and standard deviation of the GPS altitude error. The data in the tables are grouped according to two main providers, namely, the National Geospatial-Intelligence Agency (NGA) and the International Geosynthetics Society (IGS). The NGA mostly provides GPS solutions to first responders, warfighters, intelligence professionals, and policymakers (National Geospatial-Intelligence Agency, 2020). In contrast, the IGS is dedicated to the scientific and engineering development of geosynthetics and associated technologies (International Geosynthetics Society, 2020). Hence, in all conventional cases, GPS solutions employed in standard con-

Table 2.1: Yearly GPS Altitude Error - Mean (GPS.gov, 2020)

Year	**Mean**			
	IGS		**NGA**	
	No Correction	RAIM	No Correction	RAIM
2019	3.76m	2.12m	1.46m	1.45m
2017	4.98m	2.31m	1.46m	1.45m
2016	3.82m	2.09m	1.45m	1.44m
2015	10.56m	2.10m	1.49m	1.46m
2014	9.91m	2.06m	1.54m	1.48m
2013	22.91m	1.73m	1.48m	1.47m

Table 2.2: Yearly GPS Altitude Error - Standard Deviation (GPS.gov, 2020)

Year	**Standard Deviation**			
	IGS		**NGA**	
	No Correction	RAIM	No Correction	RAIM
2019	6.71m	0.14m	0.05m	0.04m
2017	7.92m	0.77m	0.06m	0.06m
2016	13.70m	0.07m	0.05m	0.05m
2015	22.91m	0.09m	0.06m	0.04m
2014	21.56m	0.11m	0.10m	0.07m
2013	281.93m	0.09m	0.05m	0.05m

sumer applications are provided through IGS stations. Furthermore, the clear differences in accuracy between the IGS and NGA solutions are mostly due to the fact that NGA solutions utilize a dual-band solution similar to an RTK-GPS. The difference is that an RTK-GPS solution uses a local base station for a reference and correction through a second solution, whereas NGA solutions would include the second solution as a different frequency in the satellite signal. The additional frequency is compared to the other signal and the differences are used for correction of the received satellite solution.

In addition, Tables 2.1 and 2.2 are subdivided into no correction and Receiver Autonomous Integrity Monitoring (RAIM). RAIM is defined as a Fault Detection and Exclusion (FDE) algorithm which uses additional redundant satellites to verify the integrity and accuracy of the triangulated position. It is

typically used in solutions where higher accuracy is required and is not widely available, as it is implemented in the GPS receiver and thus dependant on the model in use.

In summary, Tables 2.1 and 2.2 illustrate the decrease in altitude error from 2013 to 2019, hence providing motivation for the consideration of using GPS altitude measurements. As in most cases regarding an autopilot solution, a GPS module would be present in the selection of sensors of a quadcopter. However, a GPS module is typically included for the absolute lateral and longitudinal position solutions it can provide and rarely used for its elevation solution. Furthermore, the data indicates an increase in accuracy of the elevation solution and thus acts as an additional motivation for this research regarding the benefit of GPS-aided altitude estimation.

2.3 Barometeric and GPS Altitude Fusion

In this section, various methods of altitude estimation are evaluated based on the concept of barometric and GPS altitude fusion.

Zaliva and Franchetti (2014) implemented the fusion of barometric and GPS altitude by using the GPS to correct for the barometer drift and thus dynamically calibrate the barometer. Based on Maximum Likelihood Estimation (MLE), the authors derived equations for the parameter estimation of the GPS's probability distribution in the form of a pooled variance and sample mean. The estimated parameters are used to correct the variance of the barometer through ordinary least squares variance correction. Lastly, optimization of the correction is proposed as a cost function was derived to optimize the temporal window used for fusion. The cost function is minimised to determine the optimal number of previous samples that are considered for sensor fusion.

From the obtained data, the authors claim an average confidence bound reduction of 85 % for the algorithm compared to that of a GPS alone. In the review of the results, the authors illustrate the confidence bounds for a single set of data over a 200 second interval accompanied by a graph of the minimised cost function. From the confidence bounds, a difference in GPS and barometric altitude is clearly visible as expected due to the presence of drift. Visible variances in the GPS altitude did not appear to affect the final corrected altitude, illustrating the effectiveness of the algorithm.

Additionally, the authors implemented and tested the algorithm using cell phones in various environments, thus in controlled environments where sudden changes in altitude would be unlikely. While effective at illustrating the algorithm's usefulness, it is unclear on how it would perform in a dynamic system, such as a quadcopter during flight. For instance, the dependency of the altitude error, based on the size of the temporal fusion window, illustrates the

minimum error is achieved when the number of GPS samples used is between 40 to 50. As it is well known that GPS sensors have a significantly slower sample rate than that of a barometer, 40 to 50 samples could potentially describe a period of 4 to 5 seconds. In the case of quadcopter flight, significant changes could occur over such a timespan leading to inaccuracy and potentially resulting in failure or a crash. In conclusion, the authors illustrate a novel method of effectively estimating and correcting the barometer drift through the inclusion of a less accurate GPS sensor.

Contreras and Hajiyev (2019) investigated the fault tolerance capabilities of three different Kalman filter-based altimeters. These comprised of an Integrated-Baro-Inertial (IBI), an Integrated-Inertial-GPS (IIG), and an Integrated-Baro-Inertial-GPS (IBIG) altimeter. The authors implemented the three altimeters using an Optimal Kalman Filter (OKF), as well as a Robust Kalman Filter (RKF) for the purposes of testing abrupt faults. In the cases of the IBI and IIG altimeters, the implemented structure consisted of a central processing unit (CPU) and an OKF. The CPU was used to adjust for dissimilarities in the sensor's reported altitude, with the difference in output used as a measurement for the OKF. The OKF would create an estimate based on the difference and thus used as a correction to the altitude reported by the inertial altimeter. As for the IBIG case, the structure used the IBI and IIG implementations as independent local Kalman filters and combined the estimates through a fusion algorithm. The fusion algorithm used the variances of the IBI and IGI correction estimates as weights for the combination of the IBI and IIG corrections. It is to be noted that in the tested cases, the altitude measurement was determined using the inertial altimeter, with the tested combinations providing a correction to address the growing inaccuracy of inertial altitude measurements.

The study found that the RKF altimeters were more accurate compared to the OKF variants in the case where measurement faults occur. According to the authors' findings, the OKF based IBIG altimeter is preferred in a fault-free case. Hence, illustrating the fusion of barometer and GPS altitude is superior and more beneficial compared to that of a barometer or GPS alone. While of minor concern, the implemented sensors are similar in terms of accuracy as the case for the barometer and GPS, featuring standard deviations of 1 and 2.23 m respectively. Thus, it raises the question regarding the effectiveness of the proposed combinations should the sensors differ significantly. However, the authors do illustrate an effective method of fault rejection as well as the added benefits of multi-sensor fusion in altitude estimation.

Similarly, Whang and Ra (2008) implemented the fusion of air-data and GPS measurements through multiple hypothesis Gaussian approximation. The GPS measurements are used alongside the air-data to estimate and compensate for the barometer error. The authors implemented a structure that computes

the barometer altitude in addition to the estimated barometer error. Using a compensation filter, a height estimate is then determined using the barometer altitude and the estimated barometer error. The authors address the barometer inaccuracy in terms of a scale factor as well as bias, with both being estimated using GPS measurements, however, the latter also includes the use of air-data temperature measurements. In addition, an alpha-beta filter is used to address the requirement of a step-ahead prediction for the scale factor while also reducing noise from the corrected and compensated height estimate. In conclusion, the authors found that the proposed method resulted in a solution capable of more accurate height estimation compared to a GPS-only solution.

Utilising a variety of sensors, Błachuta *et al.* (2014) implemented a fusion method for the estimation of altitude and vertical velocity of a Vertical Take-Off and Landing (VTOL) platform. This comprised of a barometric pressure sensor, an IMU, GPS module, and an ultrasonic distance sensor. The authors implemented a complementary filter to estimate the barometer drift, in addition to a Kalman filter for the altitude and vertical velocity estimates. The results found that the proposed method was effective at estimating the vertical position and velocity of the platform while compensating for the growing barometric drift.

2.4 Other Methods of Measurement Fusion

In this section, relevant literature is evaluated that does not involve altitude estimation using a barometer or GPS module.

Various fusion architectures for the combination of multiple IMUs in addition to a GPS was investigated by Bancroft and Lachapelle (2011) as a potential solution for pedestrian navigation. The authors implemented three different fusion architectures, namely, Virtual IMU observation fusion, Centralised filter fusion, and Federated filter fusion. The three different architectures are evaluated in terms of accuracy and computational cost, while also assessing the fault detection capability of the measurements.

The authors found that the centralised filter or stacked filter resulted in higher accuracy compared to the reset free federated filter. In addition, the study also illustrated the increase in accuracy based on the number of IMUs. The federated filter reached a maximum accuracy with two IMUs, whereas the stacked filter increased linearly with 3 to 7 % for each additional IMU. Furthermore, the authors concluded that there was no evidence suggesting that FDE in IMU measurements would increase navigational accuracy.

A different approach was taken by Fong (2011) through the implementation of an adaptive state estimator to perform centralised measurement fusion

for lateral and longitudinal estimation. This was done by implementing a bank of parallel Kalman filters consisting of different models, in addition to a learning processor based on Bayesian estimation. The error covariance matrix of the Kalman filter was used to approximate a likelihood function to find the best-suited models. The study found that the derived adaptive state estimator resulted in better accuracy for the position, velocity, and acceleration, compared to the averaged estimates of the Multi-Band Kalman filter.

2.5 Literature Assessment

Reviewing the relevant literature, few contradictions were identified, with the first regarding the effect of temperature on the accuracy of barometric altitude measurements.

Ho *et al.* (2018) illustrated and found that temperature had little to no effect on the altitude measurements of barometers using four different smartphones. Opposing the statement is the work of Whang and Ra (2008) and Wei *et al.* (2016), in which both studies illustrated a method of temperature correction for the barometer. Further reviewing the work of Ho *et al.* (2018), the authors did mention that the tested sensors feature a compensation mechanism, thus contradicting their statement.

Hence, the assumption of temperature affecting barometer measurements should not be discarded, but rather considered as is the case in the work of Whang and Ra (2008) and Wei *et al.* (2016). While the work of Ho *et al.* (2018) is contradicting, it still illustrates the effect of sudden disturbances and the need for effective fault detection and exclusion. Furthermore, Wei *et al.* (2016) and Zhang *et al.* (2019) showed differing methods of altitude estimation and correcting INS errors using barometers. The work of Wei *et al.* (2016) is particularly interesting as it illustrates a simplistic and computationally efficient method of addressing barometer drift through differential measurements.

Reviewing Section 2.3 and the various methods of altitude estimation, a large discrepancy exists in terms of exact methods of addressing the barometric drift, in addition to the use of the GPS altitude. While most of the studies featured the use of a Kalman filter or a variant of it for state estimation, various additions exist in the form of cost functions, complimentary, and compensation filters. Comparably, all reviewed studies investigated the case where the accuracy of the barometer was superior to that of the GPS, thus illustrating only one side of the created range. Furthermore, the differences in accuracy between the barometer and GPS modules used in the studies vary, thus it is unclear regarding the potentially existing relationship in terms of the difference in sensor accuracies.

Additionally, Section 2.4 evaluates studies related to other methods of measurement fusion, thus illustrating differences in fusion architectures and the associated benefits. The work of Bancroft and Lachapelle (2011) provides some insight regarding the combination of state estimates using the covariance matrix, whereas Fong (2011) automates the process through an adaptive estimator that selects from a variety of different models. Equally informative is the finding of Bancroft and Lachapelle (2011), that the addition of multiple identical sensors with the intention of improving accuracy is largely dependent on the method of combination and does not guarantee significant improvement. In contrast to Section 2.3, the work mentioned in Section 2.4 illustrates methods allowing the use of the barometer and GPS altitude as altitude solutions, instead of corrections to the typical INS solutions.

Thus, identifying the second and most notable contradiction regarding the variety of different fusion methods and architectures used in the reviewed literature and the respective results. All studies in Section 2.3 showed a noticeable increase in the overall altitude accuracy regardless of the implemented fusion method or state estimation used. Hence, the contradiction is that no explicit solution exists to improve the altitude estimate when using both a barometer and GPS module. While one method could potentially be considered better is possible and partially supported by the work of Bancroft and Lachapelle (2011). However, the comparison of the results and effectiveness of the method is not, due to the numerous differences in methods, sensors, and test conditions

Lastly, Section 2.2 illustrates the very noticeable increase in GPS altitude accuracy over the past few years, thus acting as a good motivation for the adoption of GPS-aided altitude estimation. Furthermore, it raises the question of the potential benefit should the accuracy of GPS altitude surpass that of the typical barometer used in quadcopter altitude measurements.

In most cases, the general consumer would not have access to the superior NGA solutions, however, with the improvement in technology, newer GPS modules featuring RAIM would become more widely available, further motivating the use of GPS altitude.

2.6 Summary

The reviewed work clearly illustrates the inclusion of a GPS measurement for altitude estimation is beneficial and improves the overall altitude estimate. Furthermore, the use of GPS measurements appears to mostly be used as a correction for the compensation of the barometric drift, and not as an additional altitude measurement due to the inaccurate nature and slow sample rate of the sensor.

In most cases, the reviewed literature tested scenarios using one version of each sensor, namely, a barometer and a GPS. Additionally, the differences in the tested sensors varied for each of the evaluated studies, thus no clear relationship is visible.

The question is also raised regarding the effect of GPS altitude should the GPS sensor be more accurate in comparison to the barometer. In this case, the interest is whether the GPS would provide an increase in altitude accuracy, or whether the altitude accuracy would be compromised due to the less accurate barometer.

Chapter 3

Methodology

In this chapter, the techniques and procedures of the research are outlined, derived, and discussed. Firstly, a simulation environment is implemented and adapted to allow for the testing and analysis of the proposed algorithms. Secondly, the basis for the altitude estimation is derived and implemented in the form of a Kalman filter. Thirdly, to perform GPS-aided altitude estimation, a sensor fusion technique is illustrated and added to the single sensor Kalman-based altitude estimator. Lastly, various test cases and conditions are defined and discussed.

3.1 Simulation Environment

In the pursuit of identifying and illustrating the contribution of GPS-aided altitude estimation, a simulation environment is implemented to resemble the characteristics of real-world quadcopter flight. This is followed by the experimental verification, modelling, and simulation of the three sensors and concluded through the definition of the research assumptions.

3.1.1 Quad-Sim

A simulation environment was implemented to create a controlled environment free from external disturbances for the testing and evaluation of the proposed algorithm. This was done in Simulink through the use of Quad-Sim, a parameter-driven model for the simulation and design of quadcopter control systems (Hartman *et al.*, 2014). Quad-Sim mimics the control structure of a quadcopter in the form of a negative feedback control system as illustrated by the block diagram in Figure 3.1.

The controller receives a reference input which is compared to the output of the modelled system to determine the difference or error. The controller then uses the difference to determine the necessary control inputs for the system to rectify the error. The control inputs are fed to the system, which then

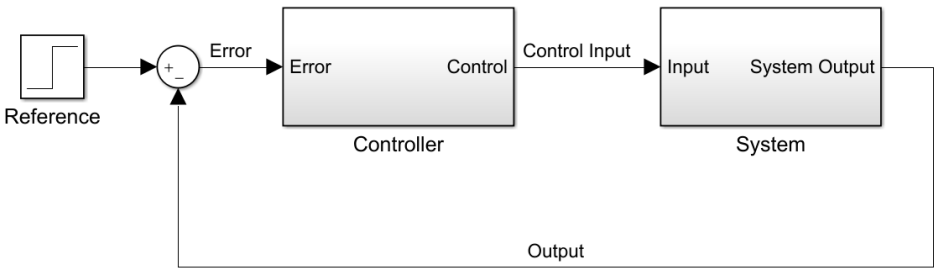

Figure 3.1: Negative Feedback Loop

changes the system state to reflect the previously received reference, after-which the loop is repeated recursively. To assess the position and movement of a quadcopter, its state needs to be defined as a set of parameters describing its freedom of movement. In the case of a quadcopter, this is referred to as the six degrees of freedom, consisting of three principal axes in addition to a rotation about each axis.

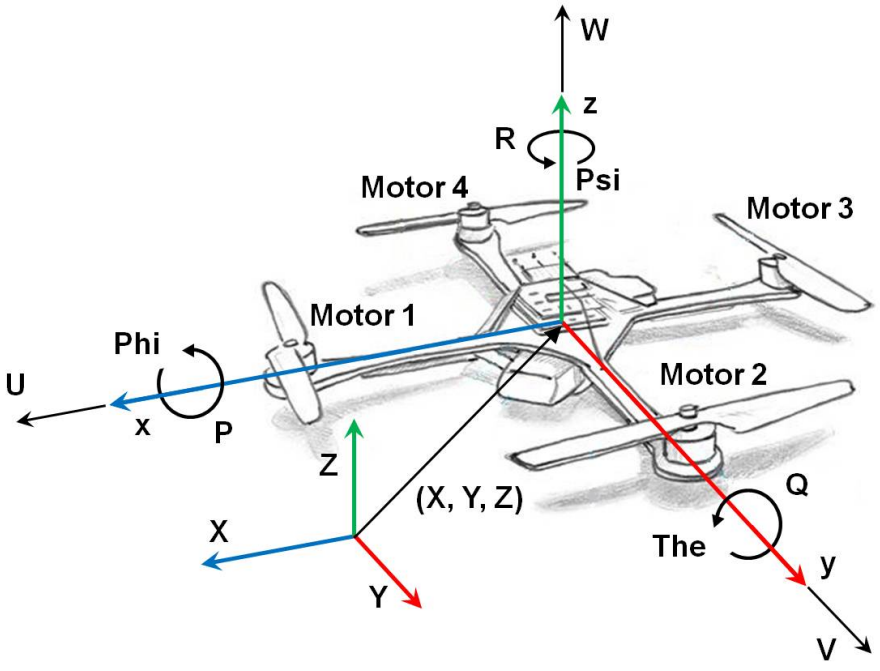

Figure 3.2: Principal Axes of a Quadcopter (Hartman *et al.*, 2014)

Figure 3.2 illustrates the three principle axes describing the translational movement, namely, the longitudinal axis (X), the lateral axis (Y), and the

normal axis (Z). Similarly, the principal rotations describe the orientation of the body or drone, with roll (ϕ) signifying a rotation about the longitudinal axis, pitch (θ) for the lateral axis, and yaw (ψ) for the normal axis. To control a system effectively and achieve stability, knowledge of the system state or output is required. In this case, the system state is described using three principal axes and rotations, thus allowing the Quad-Sim model to control and simulate the quadcopter based on a negative feedback loop as illustrated by Figure 3.3.

In Figure 3.3, the controller is made up of the Position Controller, Attitude Controller, and Control Mixing blocks, while the Quadcopter Dynamics block represents the modelled system. In the position controller, the reference input, in this case, a specified flight path, is used in addition to the system state to determine the error rotations in the body frame of the drone. Using the error rotations and the system velocity, the required roll (ϕ) and pitch (θ) commands are calculated as the attitude commands and passed on to the attitude controller.

The attitude controller determines the error and required correction for the altitude and the three rotational axes, namely, roll (ϕ), pitch (θ), and yaw (ψ). The attitude corrections are passed to the control mixing block which translates the corrections to the respective motor commands based on the motor configuration of the quadcopter, thus whether it uses an "X" or "+" frame. Moving on to the quadcopter dynamics block, the system states are to be computed using the motor commands. However, the received motor commands are in terms of a throttle percentage, which is first converted to the motor speeds, as required by the state equations. This is done through the motor dynamics block, to create realistic motor speeds for the received commands using experimental data.

Lastly, the orientation of the mobile reference frame is computed through a $Z-Y-X$ rotation matrix. In other words, the system states which represent the position and movement of the drone body are determined from the previous states by using the received motor speeds.

3.1.2 Simulated Sensors

To illustrate the benefits of GPS-aided altitude estimation, the implemented control structure of Quad-sim requires expansion. Referring to the negative feedback loop in Figure 3.1, it is clear that the output of the system is compared to the reference to determine the error.

However, in this case, the output of the system is the output seen by an observer, where in reality the output of the system is obtained using sensors. Additionally, the accuracy of the measured output that is compared to the reference is directly affected by the accuracy of the employed sensors. Furthermore, most sensors are digital and hence provide a discrete signal limited

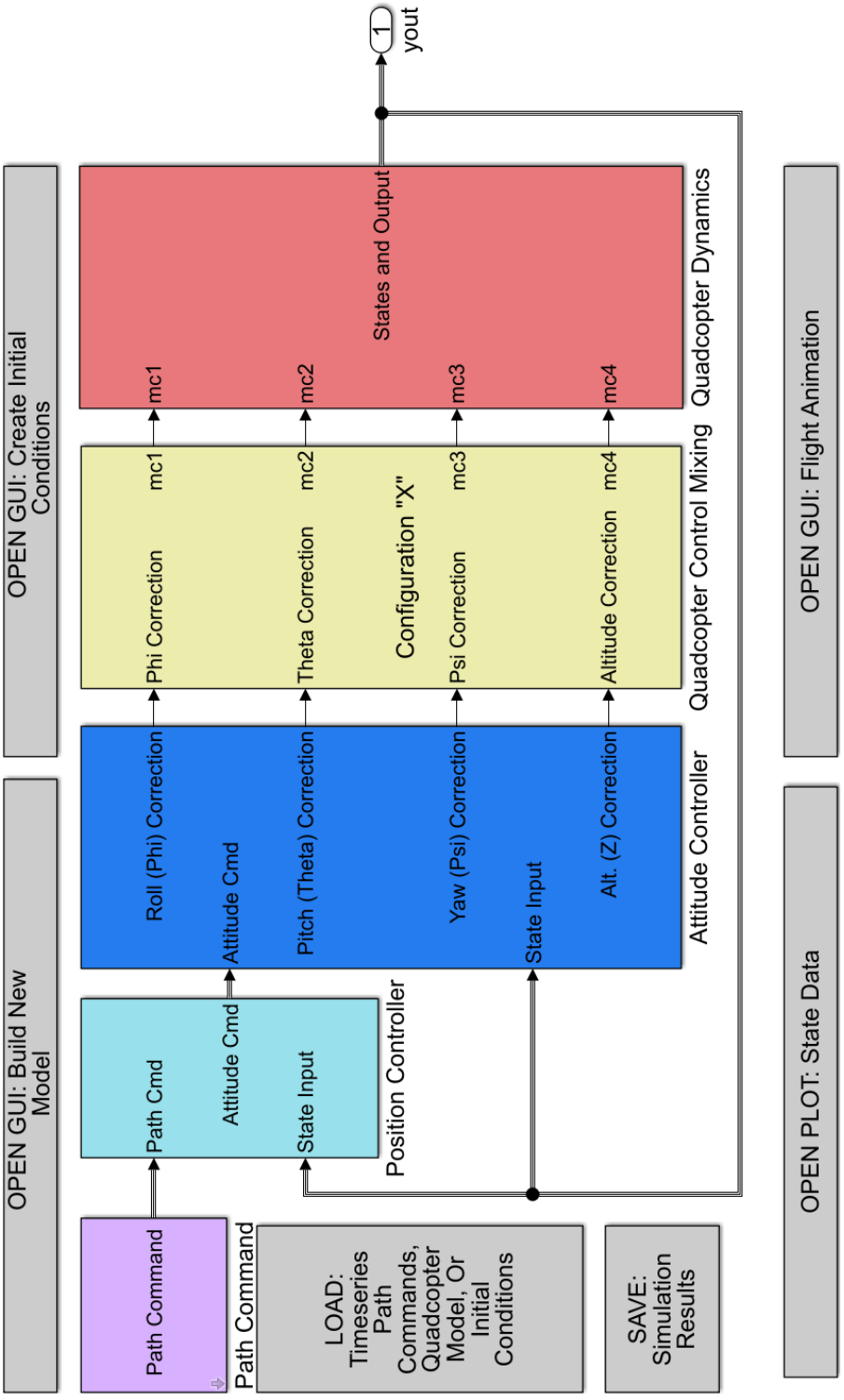

Figure 3.3: Quad-Sim Block Diagram

by the sampling speed of the respective sensor model. Consequently, in preparation for state estimation and to improve upon the Quad-sim structure to resemble the characteristics of real-world flight, a variety of sensors are to be simulated. Three different sensors were to be simulated and consist of a barometer, GPS and an RTK-GPS. The simulated sensors were modelled by using the actual altitude of the drone, in addition to a zero-mean Gaussian noise term. To further resemble the characteristics of real-world flight, the simulated sensors were to be based on actual sensors in circulation at the time.

(a) 3DR Pixhawk 1 Flight Controller (Dronecode, 2019)

(b) Piksi GNSS Module (v2.3.1) (Swift Navigation, 2016)

Figure 3.4: Selected Hardware

For the purposes of this research and availability, the 3DR Pixhawk 1 flight controller was selected along with a Piksi GNSS module from Swift Navigation as illustrated in Figures 3.4a and 3.4b respectively. The Pixhawk 1 features a variety of on-board sensors for the implementation of a working flight stack and serves as a good base as it is widely used in industry and academia (Dronecode, 2019). Regarding the measurement of altitude, Pixhawk 1 is equipped with a high-resolution barometric pressure sensor well suited as an altimeter.

As for the Piksi GNSS module, which was selected as it provides a GPS solution in addition to a more accurate and corrected RTK solution. To simulate the selected sensors, the respective noise characteristics need to be observed and determined. This was done experimentally in a controlled environment and the results are summarized in Table 3.1. The experimental procedures used in identifying and verifying the sensor noise characteristics are discussed and outlined in Appendix A.

In the case of the GPS and RTK-GPS, the simulated sensors can be described using the model in equation 3.1,

$$z_{\text{measured}} = z_{\text{actual}} + \mathcal{N}(\mu, \sigma^2) \tag{3.1}$$

Table 3.1: Sensor Noise Characteristics

Sensor	**Standard Deviation** (m)	**Variance** (m^2)
RTK-GPS	0.011	116.640×10^{-6}
Barometer	0.295	87.025×10^{-3}
GPS	5.622	31.607

where z_{measured} is the simulated sensor measurement, and z_{actual} is the actual altitude and only known to the observer. Furthermore, μ represents the mean of the probability density function, which is zero and σ^2 is the variance of the simulated sensor. The barometer was modelled in a similar manner with a small distinction. That being the inclusion of the δ term, which represents the barometer drift as shown in equation 3.2.

$$z_{\text{measured}} = z_{\text{actual}} + \mathcal{N}(\mu + \delta, \sigma^2) \tag{3.2}$$

The barometer drift (δ) was simulated as a time-dependent linear equation that was calculated from the experimentally gathered data. The simulated drift thus acts as an increasing time-dependent offset of the mean. In addition to the zero-mean Gaussian noise, the model accurately reflects the behaviour of its real-world counterpart.

3.1.3 Assumptions

To avoid external factors or phenomena from affecting the experiments and gain a better understanding of the employed algorithms, several assumptions were made. As the focus of the research is to understand and illustrate the benefits of GPS-aided altitude estimation, the priority is the accurate estimation of the drone altitude.

To ensure optimal accuracy in the altitude of the drone, the assumption was made that any translational motion on the lateral and longitudinal axes would be noise-free. In addition, any rotation about the three principal axes, vertical, lateral, and longitudinal would also be free from noise to avoid introducing unwanted inaccuracies to the vertical axis. This ensures the accuracy of the vertical acceleration used in the constant velocity model, thus avoiding additional uncertainty which could affect the results of the final estimate.

As the purpose is to improve the altitude accuracy with the intention to use the drone for heliostat calibration, the test area is to be free from obstructions. This would allow for testing without the possibility of signal loss for the GPS, potentially causing inaccuracy and affecting the results. Thus, the algo-

rithm would receive constant sensor readings without the need for additional verification or compensation.

Furthermore, it is assumed that the drone model is well implemented and that it would follow a simplistic flight path free from sudden changes in direction unless being a result of an inaccurate sensor. Thus, the system would exhibit negligible amounts of process noise, with most of the noise contribution originating from the simulated sensors.

Additionally, the effect of external disturbances is also assumed to be absent, for example, the effect of wind gusts and changes in air pressure. While these disturbances are present in real-world flight, it could directly affect the sensor readings and fall outside the scope of this research. However, it does warrant further study as disturbance rejection forms an integral part of any well-designed control system.

Lastly, the assumption is made that there is no limitation on the computational load of the implemented algorithm, and therefore requiring optimization and cost reduction.

3.2 Kalman Filter

Building upon the implemented quad-sim model and simulated sensors, a state observer is required to allow for state estimation. State estimation is required to process and filter the sensor readings to provide a more accurate estimate of the respective system states. As all sensors exhibit some form of noise or inaccuracy, variances of the measured parameters would be present even if in a controlled environment and stationary. A state estimator functions by estimating the true state of the object given the noisy measurements in addition to a predefined statistical noise term for the sensor.

3.2.1 Overview

For the purposes of the research, state estimation is to be implemented through a Kalman filter which is widely used in the control of quadcopters. The Kalman filter is a recursive estimator that alternates between two distinct phases, namely, prediction and update. In the prediction phase, the predicted state estimate and state covariance are calculated using equations 3.3 and 3.4 respectively.

$$\hat{x}_k^- = F\hat{x}_{k-1}^+ + Bu_{k-1} \tag{3.3}$$

$$P_k^- = FP_{k-1}^+F^T + Q \tag{3.4}$$

In the above-mentioned equations, the hat operator ($\wedge$) denotes an estimate of the state x, and k denotes the current time-step. Additionally, the superscripts $-$ and $+$, denote the predicted and updated estimates, respectively.

Furthermore, F signifies the state transition matrix applied to the previous state vector. B is the control-input matrix applied to the control vector u_{k-1} and Q, the process noise. In the update phase, the measurement residual, also known as the innovation, is determined using equation 3.5,

$$\tilde{y}_k = z_k - H\hat{x}_k^- \tag{3.5}$$

where z_k is the vector of current sensor measurements and H is the observation matrix. Using the predicted state and state covariance from the prediction phase, the optimal Kalman gain is calculated through equation 3.6.

$$K_k = P_k^- H^T (R + H P_k^- H^T)^{-1} \tag{3.6}$$

In equation 3.6 above, R denotes the sensor noise which is assumed to be Gaussian with a zero-mean. The updated state estimate and state covariance, equations 3.7 and 3.8, are then calculated using the predicted estimates, the measurement residual, and the optimal Kalman gain.

$$\hat{x}_k^+ = \hat{x}_k^- + K_k \tilde{y} \tag{3.7}$$
$$P_k^+ = (I - K_k H) P_k^- \tag{3.8}$$

Following the definition of the Kalman filter equations, the filter is executed recursively as part of the control loop in the described order:

1. Calculation of the predicted state estimates ($\hat{x}_k^-$);
2. Calculation of the predicted state estimate covariances (P_k^-);
3. Formulation of the innovation using the sensor readings ($\tilde{y}_k$);
4. Computing the optimal Kalman gain (K_k);
5. Calculation of the updated state estimates ($\hat{x}_k^+$) and;
6. Calculation of the updated state estimate covariances (P_k^+).

3.2.2 States

Using the implemented Kalman filter, five states are to be estimated and are as follows:

1. Barometer Altitude;
2. GPS Altitude;
3. RTK-GPS Altitude;

4. Vertical Velocity and;
5. Barometer Drift.

States one to three make up the first part of a Constant Velocity Model (CVM), namely, the position estimate along with an altitude sensor. State four is the second part of the CVM and used in the first three states for the implementation of the CVM. Lastly, state five represents the unknown barometer drift estimate and is to be used to remove its effect on the final altitude estimate.

3.2.3 Constant Velocity Model

A CVM is a dynamic model based on the assumption that the velocity of the system is constant over a timestep or a small interval, thus between two sample periods. It is implemented to allow for tracking of moving objects, in this case, being the drone. CVM forms an integral part of quadcopter flight controllers and resembles an Inertial Navigation System (INS). An INS functions on the principle of dead reckoning in which Inertial Measurement Units (IMU) in addition to a navigation processor are used to determine changes in position and velocity (Groves, 2013).

The changes in position and velocity with respect to a set of initialised values are determined through the integration of the IMU accelerometer readings. Consequently, INS accuracy can quickly deteriorate and requires constant calibration or position fixing for maintaining accuracy. Implementation of a CVM is done using a Kalman filter with two states that use IMU measurements along with an optional sensor that is state-dependent. The mentioned states represent the position and velocity of the model in a specific dimension, this case being vertical (z), as indicated by equation 3.9.

$$\begin{bmatrix} z_k \\ \dot{z}_k \end{bmatrix} = \begin{bmatrix} z_{k-1} & + & \dot{z}_{k-1}\Delta t & + & \frac{1}{2}\ddot{z}_{k-1}\Delta t^2 \\ & & \dot{z}_{k-1} & + & \ddot{z}_{k-1}\Delta t \end{bmatrix} \tag{3.9}$$

The two states, however, do not resemble the same format as the Kalman filter and need to be restructured. This is done by substituting equation 3.9 into equation 3.3, which results in

$$\hat{x}_k^- = \begin{bmatrix} I & \Delta t \\ 0 & I \end{bmatrix} \hat{x}_{k-1} + \begin{bmatrix} \frac{1}{2}\Delta t^2 \\ \Delta t \end{bmatrix} u_{k-1} \tag{3.10}$$

where $\hat{x}_k^- = \begin{bmatrix} z_k \\ \dot{z}_k \end{bmatrix}$, $\hat{x}_{k-1} = \begin{bmatrix} z_{k-1} \\ \dot{z}_{k-1} \end{bmatrix}$ and $u_{k-1} = \ddot{z}_{\text{IMU}}$.

It is worth noting that the control vector, u_{k-1}, comprises of the IMU measurement, in this case, the vertical acceleration. Additionally, the inclusion

of a CVM in a Kalman filter allows for updates of the system state between the sample times of the respective sensor in the Kalman model. As changes in the system state are limited by the sample rate of the relevant sensor, the CVM assists in the addition of minor changes to the state which are not directly related. Thus, small changes in the state which are not detected by the implemented sensor as a result of its sample rate or its relation to the relevant state, are accounted for. Table 3.2 summarizes the various sample rates and times for the sensors used in this study.

Table 3.2: Sensor Sampling Rates

Sensor	**Sample Frequency** (Hz)	**Sample Time** (ms)
IMU	200	5
Barometer	50	20
GPS / RTK-GPS	10	100

Sample frequencies obtained from the respective datasheets (InvenSense, 2013; TE Connectivity, 2017; Swift Navigation, 2016)

In the case of the barometer, altitude measurements can only be obtained every 20 ms, limited by the sensor sampling rate. However, in the case of the IMU, when run as a digital motion processor, measurements can be obtained every 5 ms at the common sampling rate of 200 Hz[1]. Furthermore, every subsequent barometer or GPS measurement acts as a position fix, effectively re-initialising the CVM by providing a new reference to avoid the growing integration errors present in INS solutions.

Hence, the inclusion of the CVM reduces the uncertainty of the system between the sample times of the barometer and/or GPS, thus allowing the assumption of negligible process noise provided the system model is accurate. As an added benefit, the inclusion of the CVM assists in maintaining system stability in the case where a sensor with a slower sampling rate is used. This is especially applicable in the case of the GPS in comparison to the barometer, by referring to the sample rates in Table 3.2. While a period of 100 ms measurements is somewhat acceptable and effective, it also describes the window in which the system state is not known during flight. This causes concern when accuracy and control of the system state are paramount as excessively slow sensor updates could lead to system instability. Hence, the CVM supplements the system in terms of stability by providing updates of the system state between the sample intervals of a slower sensor responsible for the position fixing.

[1]For simulation purposes the sample rate was set to 100 Hz by limiting the simulation step size to 0.01 s. As the increase to 200 Hz significantly increases the computational load and simulation duration with little to no improvement in overall accuracy

3.2.4 Baro Drift Estimation

As discussed earlier and depicted by equation 3.2, the barometer drift is time-dependant and acts as an offset to the mean of the normal distribution. To make an estimate of the barometer drift, a measurement of the drift is required and is achieved through a pseudo measurement at the current timestep (k), which is implemented using equation 3.11,

$$\delta_{\text{measured}} = \hat{x}^{-} - z_{\text{baro}} \tag{3.11}$$

where z_{baro} is the raw barometer measurement and $\hat{x}^{-}$ is the GPS or RTK-GPS state estimate, depending on the case. However, the pseudo measured drift would still fluctuate significantly as it is the difference between two independently and constantly varying parameters. Moreover, the barometer drift does not increase rapidly, but at a rather slow rate. Thus, to remove any unwanted fluctuations and minimise the potential degradation of accuracy of the barometer state, the pseudo measurement is to be smoothened using an exponential moving average shown by equation 3.12,

$$z_{\text{drift}(k)} = (\alpha) z_{\text{drift}(k-1)} + (1 - \alpha)\delta_{\text{measured}} \tag{3.12}$$

where $z_{\text{drift}(k)}$ is the current smoothed drift measurement, $z_{\text{drift}(k-1)}$ is the previous smoothed drift measurement and δ_{measured} is the fluctuating drift measurement defined in equation 3.11. Furthermore, α is a weighted multiplier which controls the contribution between the fluctuating drift measurement (δ_{measured}) and the previous smoothed drift measurement ($z_{\text{drift}(k-1)}$). A value of 0.999 was experimentally determined for α, as higher values would result in a smoother but delayed drift measurement, whereas lower values would result in higher fluctuations but with better responsiveness.

Additionally, the variance of the smoothed drift measurement is unknown and would change should differing GPS modules be used. To address the problem, the variance of the smoothed drift measurement is determined using a moving standard deviation and the result supplied to the Kalman filter as the measurement noise for the smoothed pseudo drift sensor. Effectively implementing a variation of an adaptive Kalman filter for the drift estimate.

The implementation of the drift estimate is similar to that of the altitude states, states one to three, but differs slightly as the CVM is not included. The current smoothed drift measurement $z_{\text{drift}(k)}$, is used as the sensor measurement z_k in the measurement residual (equation 3.5) to estimate the barometer drift, hence state five. In the two cases where the effect of drift estimation is tested, the estimated drift is used to correct the raw barometer reading used in the estimation of the barometer altitude, thus state one. The correction is done through equation 3.13, where the predicted drift estimate (state five) is added to the raw barometer reading at the current estimate.

$$z_{\text{baro(corrected)}} = \hat{x}_5^- + z_{\text{baro}} \tag{3.13}$$

This is done prior to the measurement residual 3.5, as the barometer altitude would be estimated from an altitude reading containing reduced drift. By using the exponential moving average, large variations in the estimated drift would still be present due to the differences in accuracy of the barometer and GPS used, however, the variations would be reduced. Hence, resulting in less unwanted noise on the corrected barometer readings and reducing the possible accuracy degradation of the barometer state, should the estimated drift correction fluctuate significantly. In the case where the drift is perfectly estimated and eliminated, the barometer would then resemble a similar sensor model to that of the GPS in equation3.1. In summary, the process for the estimation and correction of the barometer drift for the current timestep resembles the described execution of the Kalman filter in section 3.2.1, with minor alterations being performed in the following order:

1. The predicted state ($\hat{x}_k^-$) and covariance (P_k^-) estimates are determined from the updated estimates of the previous timestep using equations 3.3 and 3.4.

2. Depending on the test case, states two or three of the predicted estimates and the raw barometer measurement (z_{baro}) is used to calculate the pseudo drift measurement for the timestep using equation 3.11.

3. The raw barometer measurement for the current timestep is corrected using the predicted drift estimate through equation 3.13.

4. The measurement residual is determined using equation 3.5 and the respective sensor readings, thus the corrected barometer, raw GPS, raw RTK-GPS, and pseudo drift measurement.

5. From this point forward, the Kalman filter is executed in the standard fashion, by computing the optimal Kalman gain 3.6 and then calculating the updated estimates 3.7 and 3.8.

3.3 Sensor Fusion

To improve the accuracy of the final altitude estimate and illustrate the benefits of GPS-Aided altitude estimation, the state estimates are to be combined through sensor fusion. In this subsection, the concept of sensor fusion is defined and its application to this study is discussed and defined. After which, the method of sensor fusion is derived, and its implementation is illustrated.

3.3.1 Definition and Terminology

For this research, the inclusion of a CVM is not regarded or referred to as the implemented sensor fusion concept. As mentioned in Section 3.2.3, a CVM operates based on dead reckoning and thus provides accurate navigation over short periods relative to an initialised position. Thus, the inclusion of the CVM in states one to three is considered complementary to the altitude sensors responsible for the respective state estimates, as it aids in reducing the state uncertainty between the varying sample times of the barometer and the two GPS modules. The term sensor fusion could thus be better described as state fusion, as it involves the combination or fusion of two state estimates that were calculated using two different sensors. Hence, to further clarify, in this paper, the concept of sensor fusion refers to the combination of barometer and GPS/RTK-GPS altitude state estimates to formulate a combined final altitude estimate.

3.3.2 Covariance Intersection

To ensure that accuracy of the estimated states is maintained and potentially improved, the estimates need to be combined optimally. This was done using a Covariance Intersection (CI) algorithm, more commonly known as the Bar-Shalom-Campo formula (Bar-Shalom and Campo, 1986) for correlated estimates, or the Generalized Millman's Formula (GMF)(Shin *et al.*, 2006) in the case of uncorrelated estimates. "The variance of a random variable is a measure of its variability, and the covariance of two random variables is a measure of their joint variability or their degree of association" (Rice, 1995). Hence the estimate covariance matrix P_k, present in the Kalman filter equations 3.4 and 3.8, describes the state variance in relation to itself as well as the other states. The estimate covariance matrix, shown by equation 3.14, is a $n \times n$ matrix, in this case 5×5 as there are five state estimates.

$$P_k = \begin{bmatrix} P_{11} & 0 & 0 & 0 & 0 \\ 0 & P_{22} & 0 & 0 & 0 \\ 0 & 0 & P_{33} & 0 & 0 \\ 0 & 0 & 0 & P_{44} & 0 \\ 0 & 0 & 0 & 0 & P_{55} \end{bmatrix} \tag{3.14}$$

For the purposes of this study, the exact initial system states are known, and the estimate covariance matrix was initialized as a zero matrix. In equation 3.14, the diagonal entries signify the variance of the respective state estimate, while the non-diagonal entries or cross-covariances describe the variance or degree of association between two state estimates. As mentioned, the state estimates can either be correlated or uncorrelated, which can be verified using the cross-covariances of the estimate covariance matrix. In the case of correlated estimates, the cross-covariances would be non-zero, whereas being zero

or negligible values in the case of uncorrelated estimates. In this paper, the GMF is implemented as the altitude states are uncorrelated, which was confirmed as the cross-covariances converge to zero. The GMF functions similarly to a weighted average method, as the fusion weights for the combination of the states are determined using the estimate covariance matrix 3.14. For the fusion of two uncorrelated states, the fusion weights are determined using the diagonal entries of the estimate covariance matrix (Ajgl *et al.*, 2009), as shown in equation 3.15.

$$\begin{aligned} C_i &= P_{jj}(P_{ii} + P_{jj})^{-1} \\ C_j &= P_{ii}(P_{ii} + P_{jj})^{-1} \end{aligned} \tag{3.15}$$

For the fusion of the barometer and GPS, $i = 1$ and $j = 2$ are used to determine the fusion weights for states one and two of the Kalman filter. Whereas in the case where the barometer and RTK-GPS are to be fused, $i = 1$ and $j = 3$ is selected to use states one and three. Using equation 3.15 the fused state estimate is determined using the calculated fusion weights, through equation 3.16:

$$\hat{x}_k = C_i\hat{x}_i + C_j\hat{x}_j \tag{3.16}$$

where $\hat{x}_k$ is the fused altitude estimate for the current timestep. Furthermore, $\hat{x}_i$ is the barometer estimate, and $\hat{x}_j$ is either the GPS or RTK-GPS estimate depending on the test case. Similarly to the optimal Kalman gain, the estimate covariance matrix also converges to a set of values dependent on the system and system states. Thus, as the estimate covariance matrix would converge, the fusion weights would also converge to an optimal value. Hence, the variation of the state directly influences the fusion weight and consequently the contribution of the state estimate to the final fused estimate. In simpler terms, the state exhibiting the lowest variance in relation to its previous value is the more accurate state and as such would have more influence on the fused estimate.

3.4 Test Combinations and Procedures

Following the previous sections, a simulation environment has been implemented, discussed, and modified. Using the modified Simulink model, a variety of sensors have been experimentally verified, modelled, and simulated. In addition, a Kalman filter was implemented to perform the required state estimation and act as a framework for the sensor fusion based on a covariance intersection algorithm. The final modified Quad-sim environment containing the aforementioned changes is depicted in Figure 3.5 illustrating the high-level overview of the architecture. In preparation for the testing and analysis of

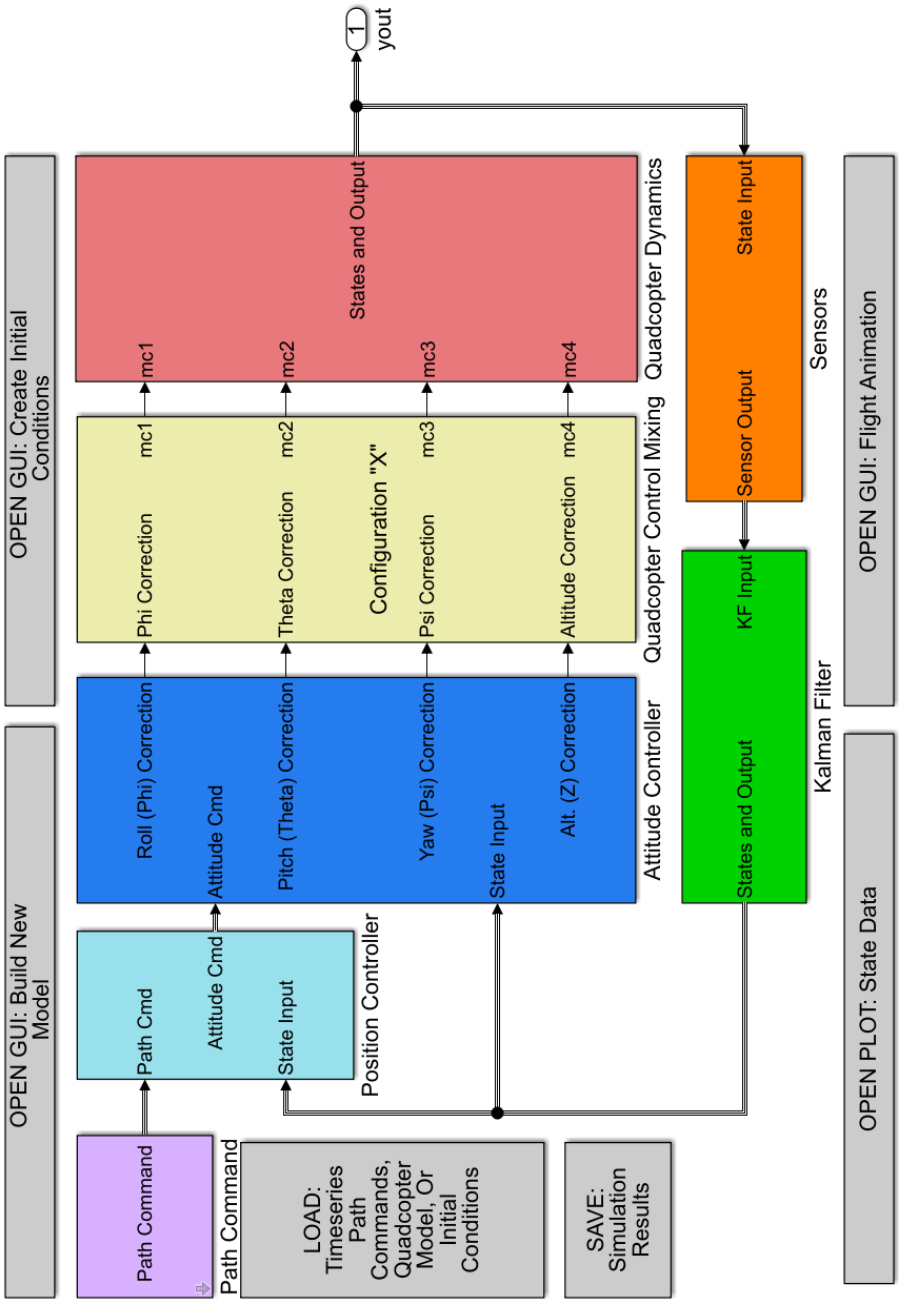

Figure 3.5: Modified Quad-Sim Environment

the developed algorithm, two different groups of test cases were outlined and discussed. The first group contains test cases based on experimentally verified, real-world sensors, whereas the second contains test cases in which a fictional GPS is combined with the barometer for a wide variety of sensor rations.

3.4.1 GPS and RTK-GPS Combinations

To illustrate the potential benefit and effect of GPS-aided altitude estimation, several sensor combinations for altitude estimation need to be tested. Using the simulated sensors defined in Section 3.1.2, seven cases were tested and evaluated, which comprised of the following:

1. Barometer
2. GPS
3. RTK-GPS
4. Baro + GPS
5. Baro + RTK-GPS
6. Baro + GPS with Drift Estimation
7. Baro + RTK-GPS with Drift Estimation

From the seven test cases, cases one to three were executed using individual sensors to act as a baseline and illustrate the various sensor-specific shortcomings and limitations. Cases four and five illustrate the benefit of a fused estimate and its effectiveness as the barometer still experiences drift. Lastly, cases six and seven illustrate the benefit of a fused estimate with the addition of correcting the barometer by using the estimated drift.

3.4.2 Sensor Noise Ratios

Referring to the sensor noise characteristics summarized in Table 3.1, a large difference in the deviation of the sensor noise can be seen between the barometer and GPS, as well as the barometer and RTK-GPS. The large difference in the two combinations is beneficial as it could illustrate the effects of the algorithm at two different ends of the range. However, due to the significant difference relative to the barometer, 19 to 1 for the GPS and 1 to 27 for the RTK-GPS, it would be difficult to illustrate any potential relationship that could exist.

As mentioned in Section 3.3.2, the fusion weights depend on the respective state variances. Thus, should one state vary significantly less than the other, it would receive a higher fusion weight and thus dominate the final estimate.

For the proposed sensor ratios, the barometer was left untouched including the simulated barometer drift as defined in Section 3.1.2. This was done intentionally as the scaling of the barometer would be more tedious considering the simulated drift, which could also add additional uncertainty. Using the sensor noise ratios of the GPS/Baro and RTK-GPS/Baro combinations as a guideline for the bounds of the range, the sensor noise ratios in Table 3.3 were selected.

Table 3.3: Tested Sensor Ratios

Sensor Ratio	**Standard Deviation**	
	GPS (mm)	Baro (mm)
1.000 : 20.000	14.8	295
1.000 : 10.000	29.5	295
1.000 : 5.000	59.0	295
1.000 : 2.500	118.0	295
1.000 : 1.875	157.3	295
1.000 : 1.250	236.0	295
1.000 : 1.000	295.0	295
1.250 : 1.000	368.8	295
1.875 : 1.000	553.1	295
2.500 : 1.000	737.5	295
5.000 : 1.000	1500	295
10.000 : 1.000	3000	295
20.000 : 1.000	5900	295

The sensor ratios were selected based on a logarithmic scale as it would span a large range in addition to the unlikelihood that the relationship of the fusion weights would be linear.

3.4.3 Test Conditions

A variety of defined cases were to be tested using the developed algorithm, and the relevant data collected and analysed. In this section, the conditions relating to the testing and evaluation of the different cases are outlined and discussed.

Firstly, the simulations were to have a duration of 1000 seconds, translating to a flight time of roughly 16 min. This was selected as the barometer would experience a total drift of 0.7 m at the end of the simulation and thus be clearly distinguishable.

Secondly, the flight path was chosen as an altitude hold, thus maintaining a constant altitude of 2.5 m for the entire duration. By using a constant value for a reference, additional inaccuracies can be avoided, for example, errors as a result of overshoot, should significant changes in altitude over a small period be required. Additionally, less accurate sensors could cause the system to settle significantly slower in comparison to that using more accurate sensors, thus causing unwanted errors.

Additionally, the drone is to start at an altitude of 2.5 m, with the motor speeds initialized at 4100 rpm to ensure that any variation in altitude would be a result of the implemented sensor. Similarly, the initial state of the drone is also accurately known, with no uncertainty, thus any deviation of the state would also be a product of the test case and the implemented sensors.

Lastly, the simulation data was logged and saved to file for comparison of the various combinations. The accuracy of the combinations was evaluated using the Root Mean Squared Error (RMSE) relative to a reference, thus the required flight height or the simulated drift, depending on the case. The RMSE was chosen as the error relative to the reference would constantly change signs and thus yield inaccurate representations of the error, while also putting more emphasis on larger errors.

Chapter 4

Experimental Results

In this chapter, the experimentally obtained results are illustrated and summarised. The results are organised into relevant sections depending on the characteristics of the tested cases.

In the first section, the GPS and RTK-GPS combinations (Section 3.4.1) are tested and the results summarised and illustrated. The results are subdivided into four different subsections, namely, single sensor, GPS-aided and RTK-aided estimation, and drift estimation accuracy. Following the first section, the results of the various sensor noise ratios outlined in Table 3.3 were also tested and illustrated. Lastly, the key observations of the experimental results are summarised in preparation for interpretation and analysis.

4.1 GPS and RTK-GPS Combinations

4.1.1 Single Sensor Altitude Estimation

In this subsection, the results of test cases one, two, and three, as defined in Section 3.4.1 are illustrated. These consist of the barometer, GPS, and RTK-GPS, respectively, with Figure 4.1 illustrating the physical altitude of the drone when using each of the mentioned sensors as its source for altitude measurements.

Firstly, and most notably, the significant difference in accuracy between the three different sensors is clearly visible. This is particularly apparent when comparing the GPS and RTK-GPS solutions. Starting with the barometer, the sensor exhibits a reasonable level of accuracy, significantly better compared to that of the GPS, however, far worse than that of the costly RTK-GPS. The main drawback of the barometer and clearly visible is its susceptibility to the growing bias or drift characterized by the constant altitude increase with respect to time. Ignoring the barometer drift, the wide adoption and use of barometers for altitude estimation is understandable, considering the low cost

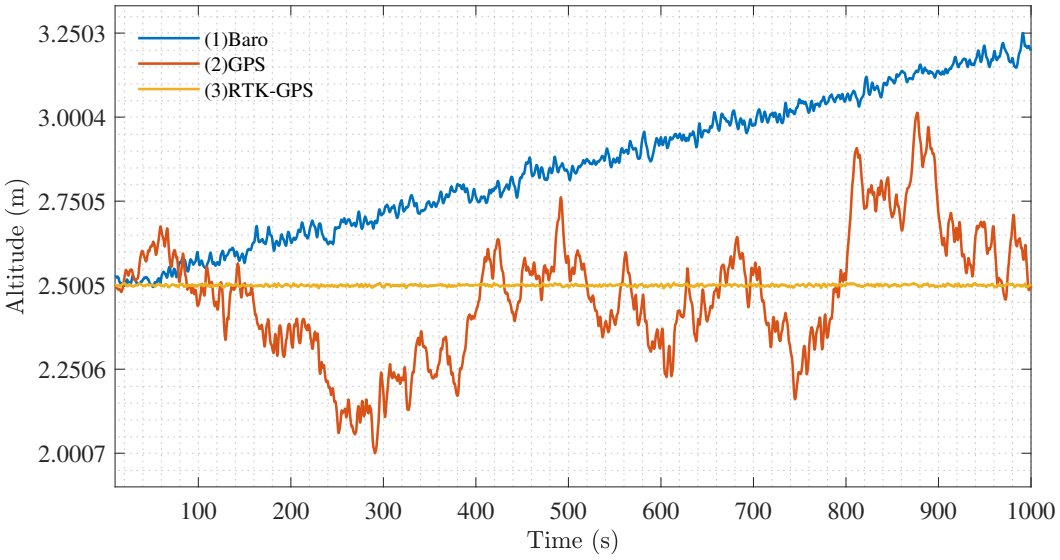

Figure 4.1: Single Sensor Altitude Comparison
The figure illustrates the accuracy of the relevant altitude sensors. Note the significant difference in accuracy between the GPS and RTK-GPS modules. Also, the effect of the constantly increasing barometer drift.

and good accuracy provided the effect of drift can be removed. Hence motivating the need for this research in addition to many methods related to the estimation and correction of barometer drift. Furthermore, the growing drift in combination with the random noise of the barometer altitude acts as a confirmation of the successful simulation and implementation of the sensor model. While the drift experienced in any real-world scenario would seldom be linear, as is this case, the simulated sensor exhibits a growing inaccuracy which can be used as a means of addressing the issue.

Moving on to the GPS, the large inaccuracy coupled with a low sample rate provides reasoning regarding the fact that GPS modules are rarely if ever, used for altitude estimation. However, the GPS does not suffer from a growing bias as is the case for the barometer, thus motivating a potential use to estimate and correct the barometer drift.

Lastly, considering the case for the RTK-GPS, it is clear that it would be very effective in estimating and correcting the barometer drift due to its superior accuracy. Of more interest is the change in overall accuracy should the barometer be used in addition to the RTK-GPS, compared to an RTK-GPS solution.

4.1.2 GPS-Aided Altitude Estimation

In this subsection, the results for the test cases utilising the standard GPS are illustrated. The mentioned cases are cases two, four, and six; in addition to the barometer case, thus case one.

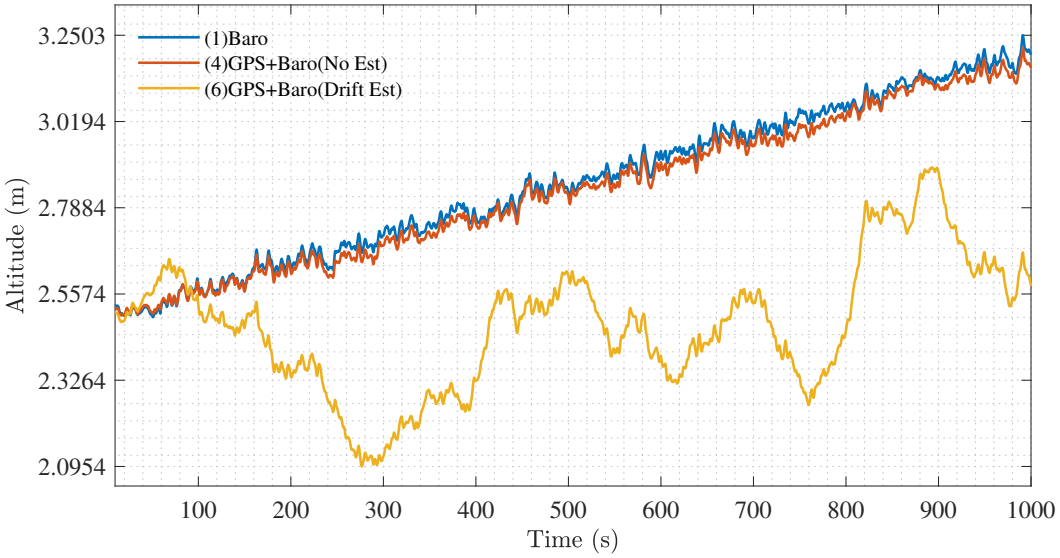

Figure 4.2: Barometer vs. GPS Fusion
Note the minimal reduction in barometer drift for the fusion case without drift estimation. Similarly, the reduction of the drift in the fusion case with drift estimation. Also, the increased variance of the altitude in comparison to cases 1 and 4

Figure 4.2, shows the physical altitude of the drone for three different test cases, namely, the barometer solution, accompanied by the sensor fusion solutions using the barometer and GPS, featuring both the inclusion and exclusion of drift estimation.

Comparing the barometer case with that of the sensor fusion case without drift estimation, minimal differences can be seen. The addition of the GPS to have a negligible impact on the accuracy of the combined solution compared to that of the barometer only. Furthermore, the effect of the barometer drift is also still clearly present and thus not effective at addressing the issue at hand. Of interest is a small difference visible between the solutions that slowly increases with respect to time. Therefore, the inclusion of the GPS altitude does appear to assist in improving the final accuracy, albeit rather marginally.

Moving on to the sensor fusion case in which the barometer drift was estimated and corrected, several differences are visible, with the first and most significant being the large variation in altitude compared to the other two cases. Secondly, the drift estimation case appears to successfully remove the

barometer drift, however, as indicated results in a less accurate solution compared to that of the barometer only.

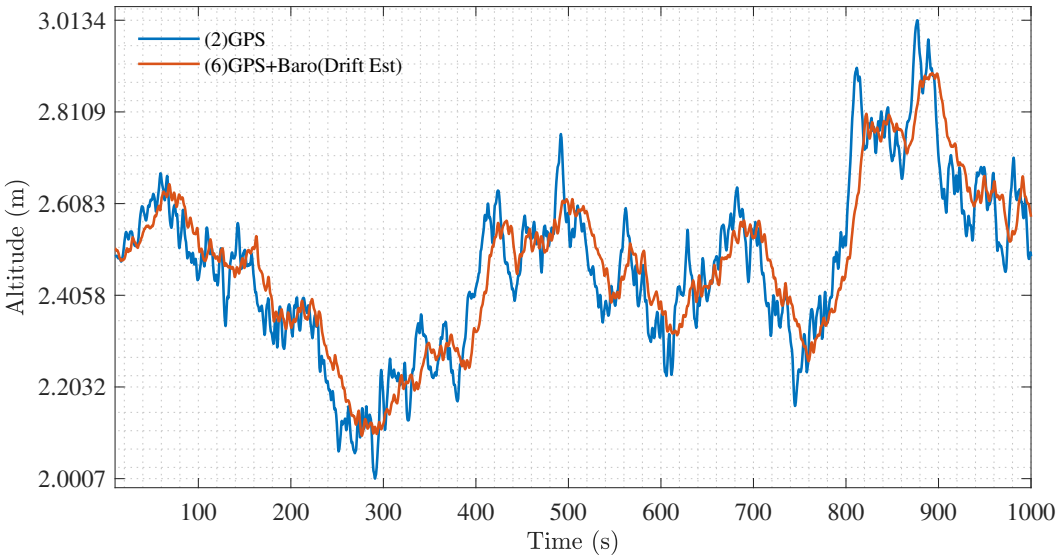

Figure 4.3: GPS vs. GPS Fusion with Drift Estimation
Note the minor improvement in accuracy compared over the GPS only case.

Lastly, the drift estimation case appears to be very similar to that of the GPS only case, however, as seen in Figure 4.3, it is slightly more accurate, as well as illustrating a slight delay in relation to the GPS only solution.

Table 4.1: GPS-Aided Altitude Error

Parameter	**Reference**	**RMSE** $(1 \times 10^{-3}\,\mathrm{m})$
GPS	2.5 m	187.4
GPS + Baro (with Drift Est)	2.5 m	174.9
GPS + Baro (with Drift Est)	GPS	12.5

Furthermore, a comparison of the two mentioned cases in relation to the required flight altitude is illustrated by Table 4.1. Regarding the required flight height of 2.5 m, a relatively small difference in the error is visible, with the drift estimation case resulting in a 12.5×10^{-3} m reduction in error compared to the GPS only solution. Finally, using the drift estimation case with the GPS only solution as a reference, a 6.7 % improvement to the normal GPS was found and could be unnoticeable on a physical system.

4.1.3 RTK-Aided Altitude Estimation

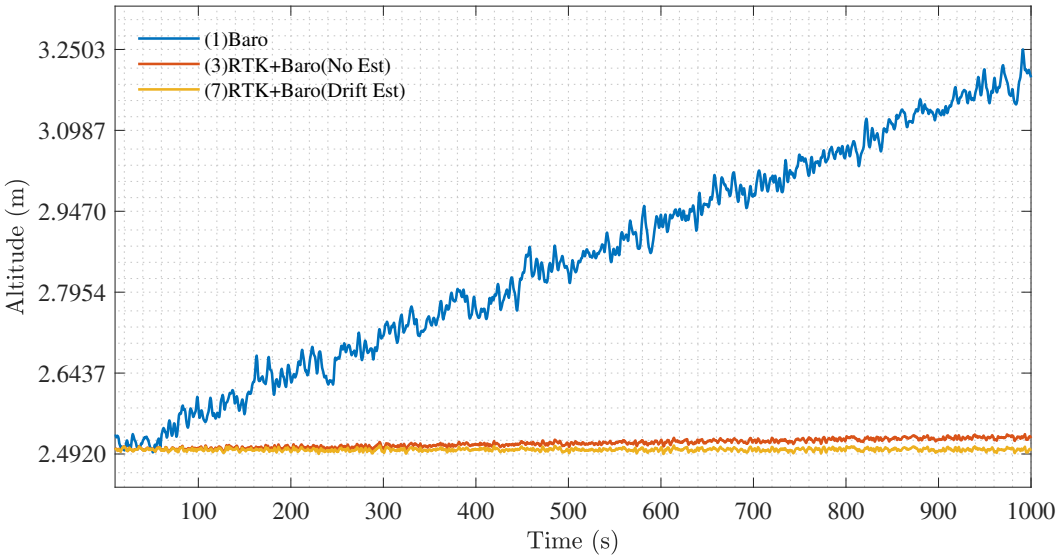

Figure 4.4: Barometer vs. RTK-GPS Fusion
Note the similarity in the fusion cases (3 and 7), in addition to the small altitude increase in case 3.

Testing and evaluating the other side of the range, where the barometer accuracy is surpassed by that of the GPS, involves the cases utilizing the RTK-GPS, with the results shown in Figure 4.4. Similar to the previous section, four cases were tested and compared, namely, the barometer only, RTK-GPS only, and the RTK-GPS fusion cases with and without drift estimation.

Referring to Figure 4.4 and comparing the barometer and the fusion case without drift estimation, a significant difference is visible. Most notably, in addition to not estimating and correcting the barometer drift, the fusion case is not as severely influenced by the barometer drift as was the case for the standard GPS. However, a small amount of drift is still present in the fusion case with no drift estimation, thus indicating that even in the case where the barometer's accuracy is surpassed by a GPS, the barometer drift still influences the final estimate.

In contrast to the GPS fusion cases, the RTK-GPS fusion cases differ very little with the only distinction being the small difference at the end of the simulation. Hence, in the RTK-GPS fusion case featuring drift estimation, the minor effect of drift has been eliminated.

The drift estimation fusion case also resembles the RTK-GPS only solution, as can be seen by Figure 4.5 and the error differences in Table 4.2. From Figure 4.5, and similar to the standard GPS case, the drift estimation fusion case is

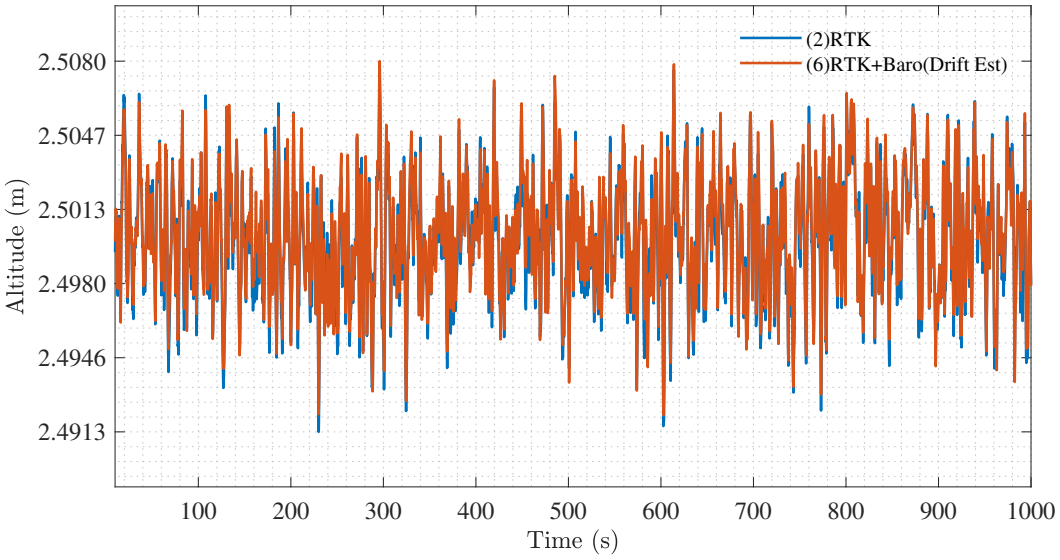

Figure 4.5: RTK-GPS vs. RTK-GPS Fusion with Drift Estimation
Note the almost indistinguishable difference and improvement of the fusion case over the RTK-GPS only case.

Table 4.2: RTK-GPS-Aided Altitude Error

Parameter	**Reference**	**RMSE** $(1 \times 10^{-3}\,\mathrm{m})$
RTK-GPS	2.5 m	2.639
RTK-GPS + Baro (with Drift Est)	2.5 m	2.589
RTK-GPS + Baro (with Drift Est)	RTK-GPS	0.050

slightly more accurate compared to the single sensor counterpart, resulting in a 1.9 % improvement. This is also apparent as indicated in Table 4.2, however, the differences between the cases are considerably smaller in comparison to the GPS cases in Table 4.1 and are considered negligible.

4.1.4 Drift Estimation Accuracy

Lastly, this subsection illustrates and summarizes the accuracy of the estimated barometer drift relating to the GPS and RTK-GPS fusion cases, thus cases six and seven. Figure 4.6 illustrates the drift error for the GPS and RTK-GPS fusion cases relative to the simulated barometer drift. From that the graph, it is clear the RTK-GPS is far more effective at estimating the barometer drift in comparison to the standard GPS.

The RTK-GPS appears to maintain a constant error with minor variations, whereas the GPS exhibits significantly larger variations. One very notable ob-

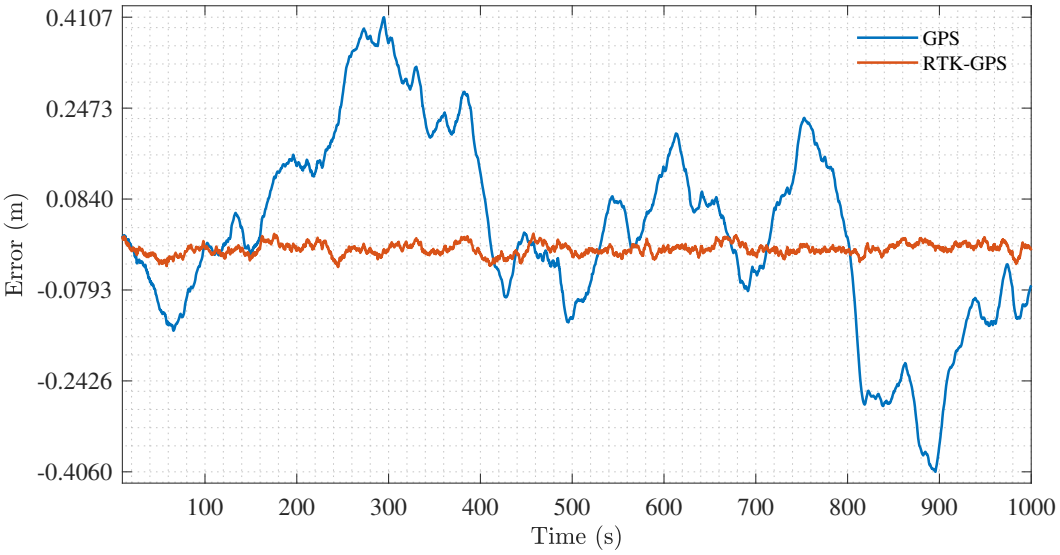

Figure 4.6: Drift Estimate Error
Observe the clear difference in error of the drift estimate relative to the simulated drift. Additionally, notice the constant minor variances in the RTK-GPS case in comparison to the larger and slower variances of the GPS case.

servation is that the GPS error variations are also remarkably slower in comparison to the RTK error variations. Furthermore, the GPS error variations resemble the same pattern as the additive inverse or the opposite of the GPS only altitude. Lastly, as the drift error varies constantly over the tested timespan, the RMSE values for the two cases were calculated to quantify the error and are shown in Table 4.3.

Table 4.3: GPS and RTK-GPS Drift Estimation Error

Parameter	**Reference**	**RMSE** $(1 \times 10^{-3}\,\mathrm{m})$
GPS	Simulated Drift	174.8
RTK-GPS		11.9

The RSME values clearly show the significant difference in accuracy between the GPS and the RTK-GPS, with the GPS error being 14 times greater than that of the RTK-GPS. Additionally, the drift estimation RMSE for the GPS is identical to the altitude RMSE for the GPS and barometer fusion case which includes drift estimation. However, contradicting the previous observation is the case for the RTK-GPS, as the drift estimate RMSE is 4.6 times larger in comparison to the fusion case RMSE.

4.2 Sensor Noise Ratios

In this section, the results of the various sensor noise ratios outlined in Table 3.3, are illustrated and reviewed. As previously mentioned in Section 3.4.2, the fusion weights used in the CI algorithm depend on the respective state variances and could result in one state dominating the final estimate should the two state variances differ significantly. In other words, should one sensor be significantly less accurate than the other, it would result in a larger state variance and thus receive a smaller fusion weight in comparison to the more accurate sensor.

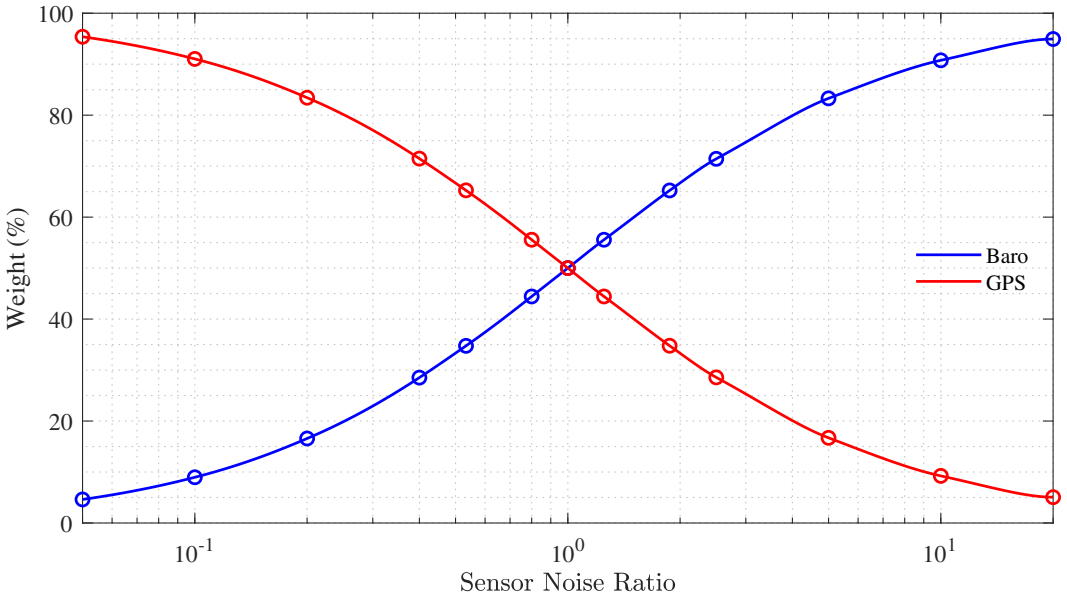

Figure 4.7: Variation of the CI Fusion Weights
Note the rapid change in the weight percentages as the sensor noise ratio moves away from unity. Moreover, notice the distribution of the weights when nearing unity. In the case of the RTK-GPS, the sensor noise ratio falls on the left-hand side and beyond the axis limits at a value of 37×10^{-3}. Similarly, in the case of the GPS, the sensor noise ratio falls on the right-hand side at a value of 19

Figure 4.7, illustrates the variation of the CI fusion weights for each of the defined sensor noise ratios. From the graph, the difference between the fusion weights changes exponentially in relation to the ratio of the sensor noise. Additionally, the graph aids verification regarding the choice of the selected ratios, as the corresponding fusion weights are sufficiently spaced in terms of the contribution percentage.

Similar to Sections 4.1.2 and 4.1.3, the altitude error for each case, relative to the required flight height, was calculated and is illustrated by Figure 4.8. The altitude error for the barometer is also illustrated, however in this case the barometer has no drift and would act as a baseline or reference for comparison.

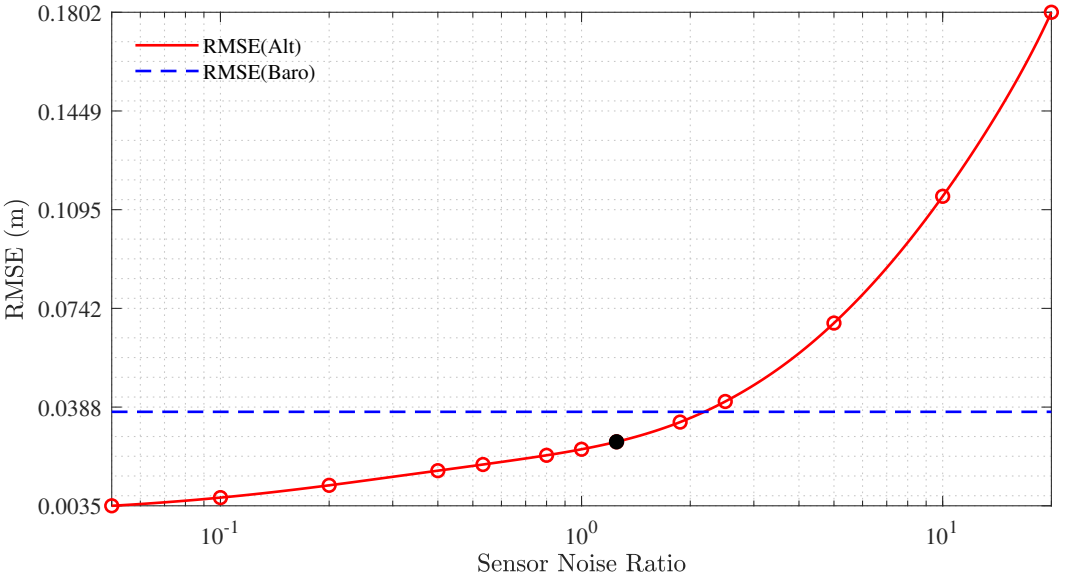

Figure 4.8: Variation of the Altitude Error with respect to the changing Sensor Noise Ratios

Observe the rapid increase in altitude error as the sensor noise ratio is increased. Similarly, notice the slow, almost linear decrease in error once the sensor noise ratio is reduced less than unity. Additionally, the blue dotted line illustrates the error for an ideal barometer with no drift, noting the intersection point with the altitude error.

As seen, the error increases exponentially as the GPS becomes less accurate. While the GPS accuracy exceeds that of the barometer, the error increases slowly and somewhat linear, whereas the exponential growth becomes more apparent near the ratio of 1.25. Thus, the GPS accuracy is 1.25 times that of the barometer as illustrated by the solid marker.

Following the same principle, the drift estimate error was also calculated relative to the simulated barometer drift and is shown in Figure 4.9. The drift estimate error resembles the same exponential nature as the altitude error, however, with a noticeable distinction. In contrast to the altitude error, the drift estimate error converges to the steady-state value near a sensor noise ratio of 0.4 indicated by the solid marker. In other words, the barometer accuracy is 2.5 times less than that of the GPS.

Lastly, Figure 4.10 illustrates the difference between the drift estimate error and the altitude error for each of the sensor noise ratios. Of interest is the three different crossover points indicated by the black markers at ratios 0.26, 1.73 and 15.00, creating four different intervals:

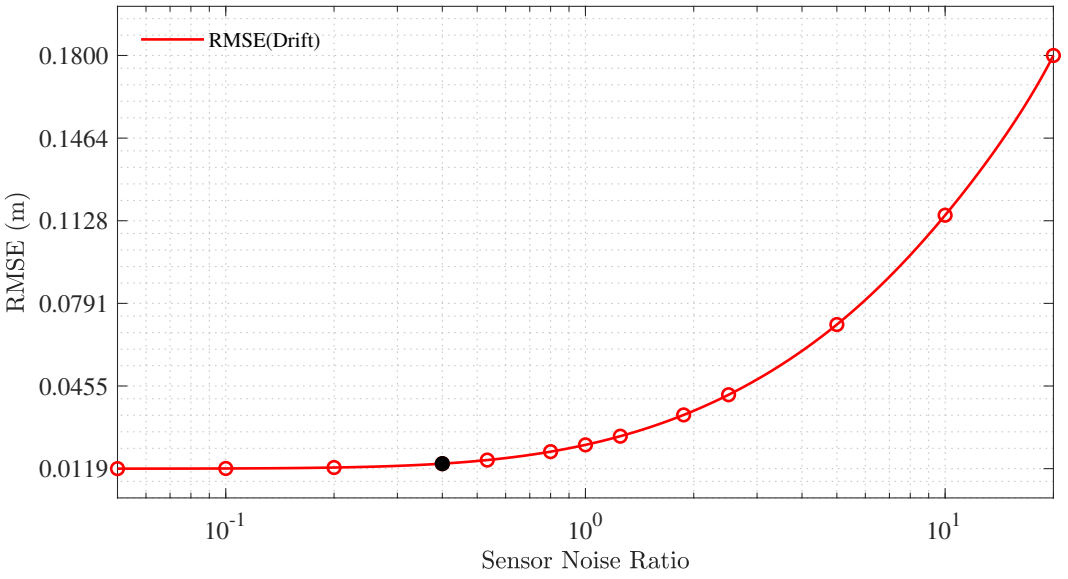

Figure 4.9: Variation of the Drift Estimate Error with respect to the changing Sensor Noise Ratios

Also note the rapid increase in error as the sensor noise ratio is increased. However, note the constant error value when the sensor noise ratio is less than 0.4.

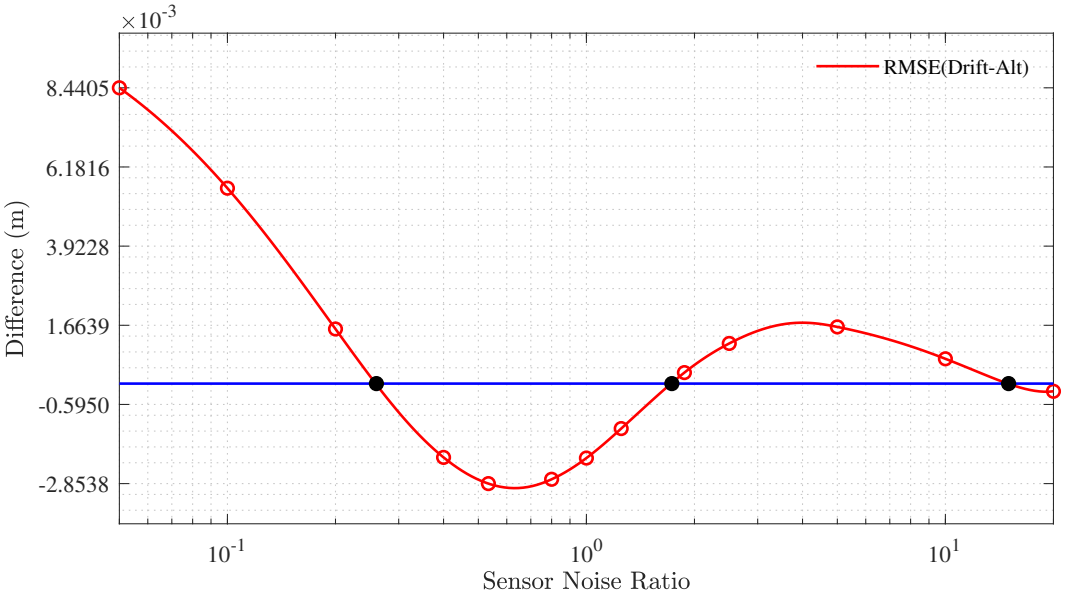

Figure 4.10: Comparison of the Drift Estimate and Altitude Error for various Sensor Noise Ratios

The figure illustrates the differences between the drift estimate and altitude errors for each tested sensor noise ratio. Positive values indicate that the altitude is more accurate and negative values indicate the drift estimate accuracy being superior. Note the differences and reversal as the sensor noise ratio is decreased towards unity. Furthermore, as the sensor noise ratio is reduced beyond unity, observe the rapid change and finally the increase following the crossover at 0.26.

$$\begin{aligned} & & \frac{\sigma_{\text{GPS}}}{\sigma_{\text{Baro}}} & < 0.26 \\ 0.26 & < \frac{\sigma_{\text{GPS}}}{\sigma_{\text{Baro}}} & < & 1.73 \\ 1.73 & < \frac{\sigma_{\text{GPS}}}{\sigma_{\text{Baro}}} & < & 15.00 \\ 15.00 & < \frac{\sigma_{\text{GPS}}}{\sigma_{\text{Baro}}} & & \end{aligned}$$

Starting with the right-hand side, thus the interval where the sensor noise ratio is greater than 15.00, the difference is negative and thus the altitude error is greater than that of the drift estimate. Additionally, the standard GPS case falls in this interval as it has a sensor noise ratio of 19.

Considering the next interval where the sensor noise ratio is between 1.73 and 15.00, the error difference becomes positive as the drift error becomes greater than that of the altitude. The difference reaches a local maximum near 5.00 as the trend starts to reverse.

Between the sensor noise ratios of 0.26 and 1.73, the difference becomes negative as the altitude error becomes greater than that of the drift. The interval reaches a local minimum between 0.53 and 0.89, when a final reversal occurs as the drift error once again becomes the larger term resulting in a positive difference when the sensor noise ratio is less than 0.26.

Lastly, the altitude error for each of the different sensor noise ratios were compared to the respective GPS only altitude error, with the differences in the error shown in Figure 4.11. From the graph, the altitude error reached a maximum difference at a sensor noise ratio of 2.50, hence the largest difference in accuracy between the GPS and the GPS fusion case, however, not necessarily the largest improvement. To determine the ratio at which the greatest improvement occurred, the altitude error difference was divided by the error of the respective GPS only case to obtain the percentage improvement relative to the reference and is illustrated in Figure 4.12. Thus, the maximum percentage improvement occurred at a sensor noise ratio of 1.25, even though the maximum difference occurred at a ratio of double the magnitude.

4.3 Summary

Using the single sensor cases, the effect of drift on the barometer was illustrated, in addition to the respective inferior and superior accuracies of the GPS and RTK-GPS modules with respect to the barometer.

Furthermore, the addition of the GPS was tested and illustrated for the sensor fusion cases with and without drift estimation. The case without drift

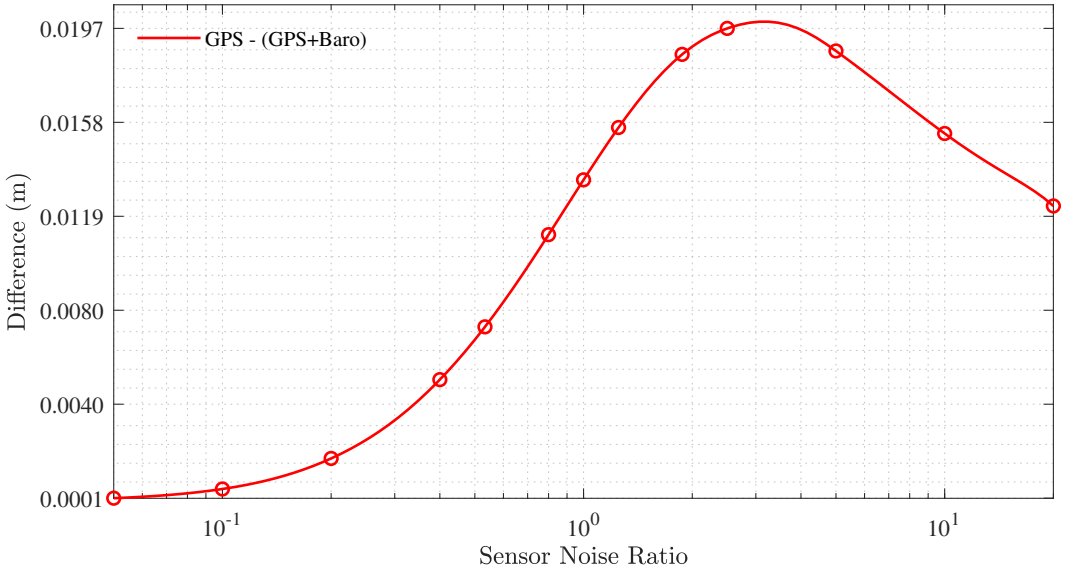

Figure 4.11: Comparison of the Altitude Error for the Drift Estimation Fusion and GPS-only Cases

The figure shows the improvement in accuracy of the drift estimation fusion case over the GPS-only case for each of the sensor noise ratios. Notice the location of the maximum difference, as well as the rapid decline as the sensor noise ratio is reduced towards and past unity.

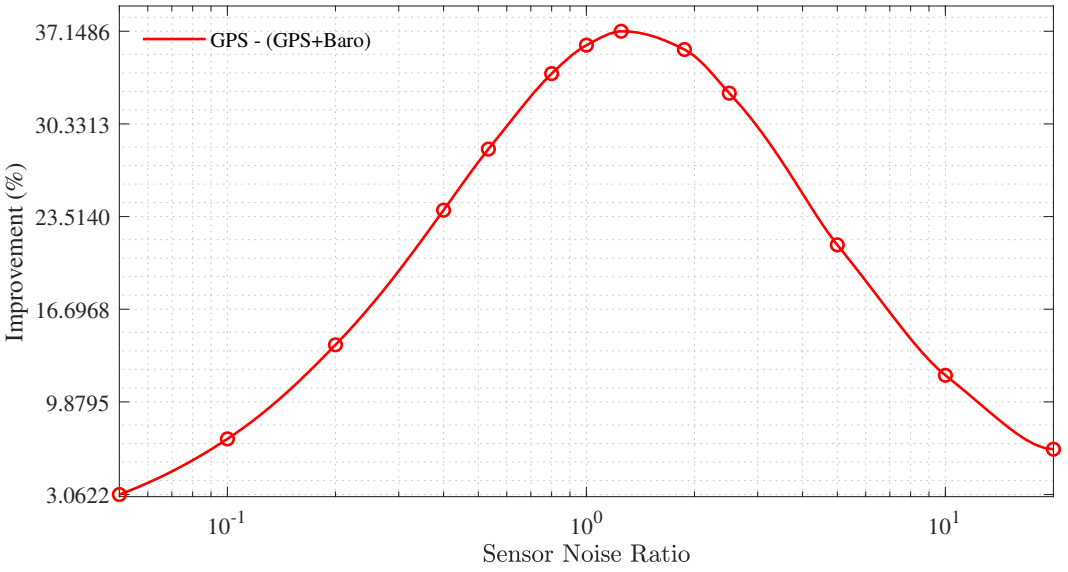

Figure 4.12: Percentage Improvement of the Altitude Error for the Drift Estimation Fusion and GPS-only Cases

The figure is similar to the difference in the altitude error for the drift estimation fusion and GPS-only cases. However, it differs, as it illustrates the percentage improvement of the error relative to the GPS-only solution. Notice the minor offset from unity for the location of the maximum point.

estimation illustrated a minimal difference in comparison to the barometer only solution. Whereas the case with drift estimation appeared to have eliminated the barometer drift, however, at the cost of a larger variance in comparison to the barometer only solution. Lastly, in comparison to the GPS only solution, the fusion case with drift estimation showed a minor increase in accuracy in addition to a small delay.

Regarding the RTK-GPS cases, the process showed similar results with minor notable differences. Firstly, the fusion case without drift estimation showed a presence of the barometer drift, however considerably less and thus opposite in comparison to the standard GPS equivalent. The RTK-GPS fusion case with drift estimation illustrated the effective removal of the barometer drift and closely resembled the RTK-GPS only solution, similar to the standard GPS case. The fusion case with drift estimation also showed a very small increase in accuracy compared to the RTK-GPS only solution, however, the difference is negligible.

The accuracy of the drift estimation for GPS and RTK-GPS fusion cases was also tested and illustrated, indicating the significant difference in accuracy between the two modules. Furthermore, the drift estimation error for the standard GPS was identical to its altitude estimation error for the fusion case involving drift estimation. In contrast, the RTK-GPS showed a drift estimation error that was 4.6 times greater than its fusion case which implemented drift estimation.

A variety of different sensor noise ratios spread over a range created by the GPS and RTK-GPS accuracies was also tested, and the results were summarized and illustrated. The tested ratios indicated exponentially increasing errors for the altitude and drift estimate as the sensor noise ratio was increased from 0.05 to 20. Additionally, the altitude error continues decreasing, whereas the drift estimate error converges to a steady-state value when the sensor noise ratio is reduced and becomes less than 0.4.

Furthermore, the difference between the errors was also calculated and illustrated four different intervals within the range of sensor noise ratios where the error difference experienced sign changes. Thus, illustrating transition zones where the altitude error would surpass the drift estimate error and vice versa.

Finally, the mean difference as well the percentage improvement of the altitude error for each of the sensor noise ratios were determined and shown. The maximum altitude error difference was found at a sensor noise ratio of 2.50, whereas the maximum percentage improvement was found closer to the middle of the range at 1.25.

Chapter 5

Discussion of Results

As previously mentioned in Chapter 1, the need to address the altitude accuracy of a drone has been identified, and a solution was proposed by including a GPS module to aid in the altitude estimation. The investigation found that in most cases quadcopters relied on a single barometer for altitude estimation and thus prone to barometer drift and pressure changes. The inclusion of a GPS module to aid in altitude estimation and correct for the unknown barometer drift could potentially improve the altitude accuracy and illustrate the benefits of GPS-aided altitude estimation.

5.1 Simulation Results

5.1.1 GPS and RTK-GPS

In this section, the results relating to the GPS and RTK-GPS test cases are analysed and interpreted. Referring to Figure 4.1, the altitude of the drone was illustrated when using a single sensor for altitude estimation. It is noteworthy that the altitudes were obtained using the Kalman state estimates for each case, thus the variations would be worse in practice should the noise parameters of the sensors be poorly approximated. The use of a barometer over a standard GPS is clear due to the large variations in altitude on behalf of the GPS. As a downside, the barometer exhibits drift, which if eliminated would result in an improvement in altitude accuracy. Thus, raising the question of whether the altitude accuracy would be improved or compromised should the GPS be used to correct for the barometer drift.

Additionally, in the case of the RTK-GPS, the barometer drift would be accurately estimated and corrected due to the superior accuracy of the sensor. However, the RTK-GPS is far more expensive than the barometer and thus it is questionable whether the inclusion of the barometer would be beneficial in comparison to only using the RTK-GPS.

GPS-Aided Altitude Estimation

Section 4.1.2 illustrates the results involving the use and inclusion of the GPS module. The sensor fusion case without drift estimation strongly resembles the barometer only solution, with the difference being a minor reduction of the barometer drift as seen in Figure 4.2. As the CI algorithm implements fusion through a weighted average based on the state covariance, the concern regarding single sensor domination is thus validated. In this case, the GPS accuracy is far less in comparison to the barometer, hence the barometer dominates the final estimate as confirmed by the fusion weights of 0.944 and 0.056. As the barometer contributes to 94.4 % of the final estimate, the presence of drift would still be clearly visible. Additionally, as the GPS would contribute very little to the final estimate, thus no noticeable change in accuracy of the final altitude would be visible. However, the 5.6 % contribution from the GPS does result in a minor reduction of the barometer drift and marginally improving the altitude estimate.

Moving on to consider the fusion case with drift estimation, the altitude accuracy is compromised by the GPS. Since the fusion weights remain unchanged, the change in accuracy is a result of estimating and correcting the barometer drift by using the GPS as a reference. As the barometer state still contributes to 94.4 % of the final estimate, the compensation for the drift is less accurate as a result of the GPS accuracy and thus influences the state and as a result the final fused estimate. Comparing the RMSE values for the GPS in Tables 4.1 and 4.3, the values are considered identical. Indicating that the accuracy of the altitude estimate is limited by the accuracy of the drift estimate and thus a result of the GPS accuracy. Additional confirmation is given by Figures 4.3 and 4.6, with the former illustrating the resemblance between the drift estimation fusion case and the GPS only solution. The latter shows the drift estimate error, which resembles the additive inverse or opposite, of the GPS only solution shown in Figure 4.1.

The results confirm that the GPS does compromise the altitude accuracy in comparison to the barometer only solution. Additionally, the fusion case with drift estimation showed an increase in accuracy of 6.7 % over the GPS only solution, thus being a potential result of the inclusion of the barometer. Furthermore, while the GPS is capable of estimating and correcting the barometer drift, albeit inaccurate and inadequate, the results suggest a correlation and warrant further investigation.

RTK-GPS-Aided Altitude Estimation

Evaluating the other side of the range, there are the test cases involving the use of the RTK-GPS as seen in Figure 4.4. Considering the sensor fusion case

without drift estimation, the results show a relationship similar to the identified single sensor domination case for the standard GPS, however, in this case, the final estimate is mostly reliant on the RTK-GPS. In the test case, the fused estimate is significantly more accurate than the barometer only solution, however a small presence of drift is still visible. Although the fusion weights resulted in 0.03 and 0.97, favouring the RTK-GPS, the need to estimate and correct the barometer drift is clear.

Considering the fusion case with drift estimation, the barometer drift is accurately estimated and corrected as expected. Comparing the fusion case with the RTK-GPS only solution in Figure 4.5, a negligible improvement can be seen, indicating that in this case, the fusion with the barometer, in addition to the drift estimation is not beneficial. Additional confirmation is given by Table 4.2, as the fusion case resulted in a 1.9 % improvement over the RTK-GPS only solution.

Examining the drift estimation accuracy in Figure 4.9, it is clear that the RTK-GPS is effective at estimating the barometer drift, as the variance is of a small magnitude with minor fluctuations in comparison to the GPS. However, when comparing the drift estimation error with the altitude error in Tables 4.2 and 4.3 respectively, it can be seen that the altitude accuracy is no longer affected by the accuracy of the drift estimate. In this case, the drift estimate error is 4.6 times greater than the altitude error, suggesting a potential crossover point existing in the range created by GPS and RTK-GPS.

Summary of the GPS and RTK-GPS Findings

The GPS and RTK-GPS tests revealed several insights while also raising new questions. Firstly, the case for sensor fusion without drift estimation was proved to be ineffective as both single sensor dominance cases indicated the presence of drift and thus inaccuracy.

Continuing with the case of single sensor dominance, and fusion with drift estimation, both ends of the range being the RTK-GPS and GPS, illustrated an increase in accuracy over the relevant GPS only solution. Thus, based on the concept that two overlapping measurements would provide a more accurate combined reading in comparison to the individual readings. As the addition of a second reading reduces uncertainty, the magnitude is largely dependent on the difference in accuracy of the two sensors, in other words, the ratio. Thus, the benefit of fusion through the CI algorithm is indicated, as both cases showed an increase in accuracy, regardless of whether the altitude error was dependent on the drift estimation error.

Furthermore, as the results suggest that the altitude error is affected and potentially dependent on the drift estimation error, the use of the GPS for drift estimation is deemed ineffective, as it compromises the final estimate in the tested case. On the other end of the range, the RTK-GPS was extremely effective at addressing the barometer drift, however, the inclusion of the barometer is deemed as illogical, due to the negligible increase in accuracy versus the increased computational load.

The significant difference in accuracy between the GPS and barometer, as well as the RTK-GPS and barometer, is useful for indicating the benefits and effect on either side of the range. However, it is also problematic, especially in identifying a potential transition point where the altitude accuracy is no longer equal in magnitude to that of the drift estimate accuracy. Additionally, both cases exhibited single sensor dominance, thus the effect of its absence is unknown and requires investigation.

5.1.2 Sensor Noise Ratios

To address and avoid the case of single sensor domination, a variety of sensor noise ratios were selected as mentioned in Section 3.4.2, and the corresponding fusion weights for each case are indicated in Figure 4.7. The various ratios indicate different levels of contribution to the final estimate, thus avoiding domination and potentially providing insight to any underlying relationships.

Reviewing the altitude error for each of the sensor noise ratios, an exponential increase in error was identified as the GPS becomes less accurate in comparison to the barometer. If the GPS is significantly less accurate in comparison to the barometer, a high sensor noise ratio is obtained and the combination leans toward the right-hand side of the range as seen in Figure 4.8. As was the case for the standard GPS, which yielded a sensor noise ratio of 19, thus having a large altitude error.

However, in that case, should the sensor noise ratio be reduced by a small factor, a significant increase in altitude accuracy could be achieved. Thus, indicating that larger sensor noise ratios quickly deteriorate the altitude accuracy and should be avoided. Additionally, sensor noise ratios less than unity results in negligible increases in accuracy as the ratio decreases. Thus, the benefit of fusion with drift estimation rapidly decreases once the GPS accuracy surpasses that of the barometer.

Furthermore, the altitude error of the barometer is also visible in Figure 4.8, however, without any drift. Thus, when the altitude error becomes less than that of the drift-free barometer, the specific fusion case provides a better solution in comparison to an ideal drift-free barometer. In this case, the crossover occurs at a sensor noise ratio of 2.1, indicating that the fusion case

with a GPS that is half as accurate as the barometer, would provide an altitude accuracy similar to that of the ideal barometer.

Evaluating the case for the drift estimation error seen in Figure 4.9, a similar exponential relationship is visible with a minor distinction. The drift estimation error converges to a steady-state value at a ratio of 0.4, indicating a limitation on the accuracy of the drift estimate. Thus, it would no longer be beneficial to estimate the barometer drift should the GPS accuracy be greater than 2.5 times that of the barometer.

As derived in Section 3.2.4, the drift is estimated using the Kalman filter in addition to the pseudo measurement. The accuracy of the drift measurement depends on the accuracy of the reference, thus the GPS state, in addition to the raw barometer measurement. As the accuracy of the barometer measurements remains constant over the tested range, the accuracy of the GPS state would increase as the sensor noise ratio is decreased, and thus should not cause a limitation. Thus, through deduction, the limitation would then occur due to the Kalman filter, effectively achieving its maximum accuracy for estimating the drift given the pseudo measurement and noise of the barometer. Similar to the case for the altitude error, the drift estimate error also rapidly increases with larger sensor noise ratios and thus could affect the final estimate as was the case for the standard GPS.

In the GPS case, the drift estimate and altitude accuracy were identical, in addition to the fusion case closely resembling the GPS only case. Whereas for the RTK-GPS, the drift estimate and altitude accuracy differed significantly, similarly, the fusion case also resembled the RTK-GPS only solution due to the 1.9 % difference. The assumption was made that the drift estimate and altitude accuracies are correlated and that a crossover exists where the altitude accuracy improves noticeably in comparison to the drift estimate accuracy. From the drift estimation error in Figure 4.9, it is somewhat verified since the error converges to a steady-state value, while the altitude error would continue reducing.

However, when comparing the difference in the drift estimate and altitude errors in Figure 4.10, a more complex behaviour can be seen. Positive values indicate the altitude estimate is more accurate, whereas negative values indicate a higher accuracy on behalf of the drift estimate. Furthermore, the gradient would indicate the rate of error change of the two parameters. A positive gradient thus indicates that the drift estimate error is experiencing larger changes in comparison to the altitude error and vice versa.

Thus, gradients near zero indicate similar and equal changes in the drift estimate and altitude accuracy, as was the case for the standard GPS at a sensor noise ration of 19. The positive gradient between 0.6 and 4, indicates the drift estimate accuracy improving faster in comparison to the altitude accuracy, with the drift estimate becoming the more accurate of the two when the

ratio is lowered past 1.73. Furthermore, the fusion case also reached better accuracy in comparison to the ideal barometer at 2.1, which is in the same interval. Thus, in other words, the fusion of the barometer and a GPS that is half as accurate as the barometer results in a more accurate solution than the ideal drift-free barometer. Both the drift estimate and altitude errors increase significantly past a sensor noise ratio of 5, falling outside the positive gradient interval. Additionally, on the left-hand side of the positive gradient interval, the drift estimation error nears a steady-state value, while the altitude error shows negligible decreases. This potentially signifies a correlation between the accuracy of the altitude and the drift estimate over the positive gradient range of 0.6 and 4.

Lastly, the difference between the fusion cases with respect to the relevant GPS only solution can be seen in Figure 4.11. The fusion case reached the largest difference with respect to the GPS only solution near a ratio of 3, thus also within the identified positive gradient interval, yet prior to the 2.1 ratio indicating the ideal barometer performance.

However, as mentioned in Section 4.2, the largest difference does not guarantee the largest improvement, as illustrated by Figure 4.12. The Largest improvement relative to the GPS only solution was reached near 1.25, thus within the positive gradient interval for the altitude and drift error difference. Additionally, less than the 2.1 ratio for the ideal barometer accuracy, as well as just prior to the point where both the drift estimate and altitude errors begin to see minor reductions in error when the sensor noise ratio is reduced.

5.1.3 Key Findings

From the conducted tests and interpretation of the results, a variety of discoveries were identified illustrating the benefits of GPS-aided altitude estimation.

From the GPS and RTK-GPS cases, it was illustrated that neither case was effective or beneficial. In the case of the GPS, the drift estimation would compromise the accuracy of the final altitude estimate as a result of the poor accuracy of the GPS. Similarly, was the case for the RTK-GPS, in which the fusion case with drift estimation saw a minimal increase in accuracy and thus impractical due to the increase in computational load. Both cases were identified as illustrating single sensor dominance, in which the final estimate closely resembles a single sensor and is largely dependent on it. This was due to the large difference in accuracy between the relevant implemented GPS modules and the barometer. The tested cases also evaluated the use of sensor fusion without drift estimation, indicating the need for drift estimation as the barometer drift was present even when the fused estimate was dominated by the RTK-GPS.

Evaluating the various sensor noise ratios, a variety of relationships were identified based around the concept noise ratios between the barometer and GPS. The altitude error of the final estimate was found to increase exponentially as the sensor noise ratio was increased. As the sensor noise ratio is lowered, the altitude error is reduced significantly, however, the improvement in accuracy reduces as the ratio becomes smaller, with ratios less than one illustrating minor improvements and thus not beneficial.

Similarly was the case for the drift estimation error, however, the drift estimation error converges and illustrates a maximum accuracy, thus indicating that estimating the drift when the sensor noise ratio is less than 0.4, would not result in a more accurate drift estimate. Furthermore, for the fusion case to exhibit an accuracy on par with that of an ideal barometer, thus featuring no drift, the sensor noise ratio should be less than 2.1 and acts as part of an ideal setpoint.

Comparing the drift estimate and altitude errors revealed a complex dynamic relationship. However, an optimal range was identified, characterised by the positive gradient between 0.6 and 4, as the drift estimate error reduces at a faster rate in comparison to that of the altitude as the sensor noise ratio is decreased. Several key points were found to fall within this defined interval and thus assist in illustrating its relevance.

Firstly, the interval ends just prior to the point where the drift estimate error converges, thus at 0.4. Secondly, in comparison to the relevant GPS only solution, the maximum percentage improvement for the fusion case was found to occur at 1.25. Thirdly, the altitude error starts to decrease linearly near a ratio of 1, thus illustrating minor improvements. Lastly, the ideal barometer accuracy at 2.1 also falls within the defined interval as well as being near its centre point.

5.2 Relevance and Significance

The results and findings indicate that GPS-aided altitude estimation is beneficial, however, given certain conditions. Thus, illustrating the use of GPS modules in altitude estimation, to function as an additional altitude measurement, but also and most importantly for correcting the unknown barometer drift. The study also illustrated an optimal interval in which the largest benefit of the proposed algorithm could be achieved and assists in understanding the complex relationship.

Comparing the findings with previous studies confirms that the inclusion of a GPS for altitude estimation is beneficial and leads to an increase in accuracy. However, all evaluated studies varied in terms of the methods employed, sensor accuracy, and method of analysis.

The work of Zaliva and Franchetti (2014) indicated a 85 % reduction of the confidence bounds for the combined altitude with respect to the original GPS. Additionally, the author tested two combinations which would yield sensor noise ratios of 10 and 29, which partially confirms the tested results. As a sensor ratio of 10 would exhibit a noticeable improvement and could be effective, however not so for the case of a ratio of 29. Similarly, Whang and Ra (2008) also came to the same conclusion, with a sensor noise ratio of 14. The inclusion of a GPS resulted in a solution more accurate than that of the GPS only, and thus also in accordance with the simulation results.

Furthermore, Contreras and Hajiyev (2019) tested various combinations of altimeters with sensors yielding a sensor noise ratio of 2.23, and found that each had differing strengths and weaknesses, with the barometer and GPS based optimal Kalman filter yielding the best result in the fault-free case. Thus, supporting the findings that the various sensor fusion cases resulted in better accuracy in comparison to the single sensor cases. While none of the studies investigated the case where the GPS accuracy would surpass that of the barometer, the results indicated a negligible benefit, potentially confirming the absence of relevant available information.

Lastly, with the increase in accuracy of GPS sensors, as illustrated in Tables 2.1 and 2.2, the sensor noise ratio would reduce provided the barometer remained unchanged. Thus, as the ratio would be large, as was the case for the standard GPS, a minor increase in GPS accuracy would result in a noticeable increase in altitude accuracy.

The results and findings are similar to previous studies that illustrated the improvements and benefits of the proposed methods. However, different from previous studies, the results also indicate an underlying relationship for the proposed method. Thus, providing insight into the potential benefits and compromises, depending on the case, in addition to illustrating a range for optimal benefit.

5.3 Limitations

It is noteworthy that the exact methods of implementation outlined in this research apply to the relevant case, where the focus is on illustrating the benefit of GPS-aided altitude estimation. Thus, to further clarify, differences in the implementation of the control structure and execution could be present as it was required for the purposes of simulation.

Firstly, the experiments were limited to simulations, allowing for repeatably in a controlled environment, which would have been impossible in a real-world case. Testing and evaluation of the developed algorithm in a real-world sce-

nario could yield different results and is required for additional confirmation of the collected results and findings.

Secondly, and thus related to the previous, is the exclusion of external disturbances and the imposed effect on the system. Hence, the uncertainty in the system was minor and aided in testing an effective model without the need for case by case tuning of the Kalman filter, which could compromise the results as numerous variables would differ between the tested cases. However, the work of Contreras and Hajiyev (2019) does provide some insight into the disturbance rejection qualities of similar designs, providing some assurance.

Thirdly, the tested algorithm is somewhat computationally intensive and could thus be problematic when trying to implement it on a real system. However, the algorithm was derived without a limitation on the computational load, and thus could be reduced, for instance, the removal of the RTK-GPS state. Furthermore, the barometer and velocity states would replace the altitude and vertical velocity states in the Kalman filter of the real-world model, thus only requiring two additional states, namely, the GPS altitude and drift estimate states.

Lastly, the test involved the use of a single barometer, thus different barometers could provide different results. Additionally, the barometer drift was simulated to be linear in nature for the sake of simplicity, however, rarely is in practice. While the drift might not be linear, it should still increase at a slow rate and thus be predictable allowing for estimation.

While the mentioned limitations are notable and require investigation, it does not invalidate the findings of the conducted research but would assist in further confirmation.

5.4 Recommendations

As mentioned in the previous sections, one limitation is that the algorithm was tested using simulations, and thus an evaluation of a real-world scenario is required.

The tested cases used a generalised approach to tuning the Kalman filter, to avoid unintentional changes in accuracy, potentially compromising the results and thus the identified relationship. From the results, the cases with large differences in the sensor noise ratio were ruled out and an optimal interval was identified.

However, in the real-world case, additional tuning of the Kalman filter could result in improved accuracy, as it is case-specific and thus requires additional testing and evaluation. Thus, it is recommended to test cases that fall within the identified range of 0.6 to 4, in a real-world scenario, while also

implementing additional case-specific tuning.

Furthermore, the ability of the developed algorithm to handle disturbances also requires testing. Additionally, the Kalman filter could be altered to use dynamic values for various sensor noises. Thus, by measuring the various independent sensor measurements over a moving interval during flight, the variance of the respective sensor can be obtained and provided to the Kalman filter. This would result in an adaptive variant of the Kalman filter, which, in addition to dynamically changing the optimal Kalman gain with respect to the measurement variance, would also affect the CI fusion weights. Hence resulting in a method of dynamic fusion as well, potentially improving the final altitude estimate, while also illustrating traits of error rejection.

Additionally, improvements can also be made to potentially increase the accuracy of the drift estimate. For instance, collecting the barometer readings in a controlled environment to create a profile of the barometer drift. The profile can then be used in the Kalman filter as a reference for the estimated drift, as the difference between the estimated drift and the profile should converge to a value near zero with time.

Similarly, the same concept can be applied based on the work of Wei *et al.* (2016), to use a reference barometer to obtain differential measurements. Changes in altitude of the reference barometer would describe the drift, which could be used for verification of the estimated Kalman drift state.

Lastly, the problem concerning the computational load could be addressed using a base station which would perform the necessary calculations and periodically transmit updates and corrections to the drone.

Chapter 6

Conclusion

Following the objectives of the research, a simulation environment resembling quadcopter flight was implemented, in addition to the simulation of the relevant to-be tested sensors. A method for state estimation was implemented using a Kalman filter and sensor fusion accomplished through combination based on covariance intersection.

A variety of test cases were evaluated relating to the use of a GPS and RTK-GPS, alongside a barometer in a combination of single sensor cases, sensor fusion, and drift estimation cases. The results showed a limitation due to the large difference in the accuracy of the two GPS modules in relation to the barometer. In the case of the GPS, the altitude accuracy was compromised and thus not suitable for correcting the barometer drift. Regarding the case of the RTK-GPS, the improvement in accuracy by including the barometer and correcting the drift was found to be negligible and impractical, considering the increased computational load.

Lastly, a relationship for the optimal combination of a GPS and barometer, with the purpose of altitude estimation was investigated and illustrated. The results indicated that the inclusion of a GPS for altitude estimation is beneficial, however, it is case dependent based on the difference in accuracy relative to the barometer.

The identified relationship showed notable increases in the altitude accuracy as the ratio of the GPS and barometer accuracy is decreased. Cases where the accuracy of the GPS would surpass that of the barometer illustrated minimal increases in accuracy and thus were not beneficial. An optimal interval was identified to show the maximum benefit regarding the combination of the two sensors, with the accuracy of the combined solution surpassing that of an ideal drift-free barometer when the sensor noise ratio is decreased beyond 2.1.

The results illustrate the underlying relationship of the GPS and barometer fusion and thus provide insight regarding the benefits of GPS-aided altitude es-

timation. The identified relationship also acts as a guideline for future research, by providing some insight into the possible expected accuracy improvement, as well as a potential method for comparing the results of different studies.

Appendices

Appendix A

Experimental Identification of Sensor Noise Parameters

A simulation environment resembling real-world quadcopter flight is to be implemented and as mentioned in Section 3.1, it is to be done through the Quad-Sim model in Simulink. For this research, the simulated sensors are to be based on a Piksi GNSS module, in addition to a Pixhawk 1 flight controller featuring a MEAS MS5611 Barometric Pressure Sensor. Furthermore, the respective data sheets are ambiguous, with the Piksi GNSS not indicating a reported accuracy and the MS6511 not describing the bias or drift. Thus, for verification and in preparation for the modelling and simulation of the mentioned sensors, the noise characteristics are to be experimentally determined.

A.1 Piksi GNSS Module

The Piksi GNSS module is a GPS module capable of providing standalone GPS solutions, as well as a differential or RTK solution. To provide a RTK solution, two Piksi receivers are required, with one acting as a base station while the other acts as the rover. The base station is to remain stationary and is to be initialised so that an accurate position fix can be determined.

The base station receiver was set up in the middle of a cricket field to avoid obstructions and ensure a sufficiently clear view of the horizon. The base station was powered up and left for 40 min to initialise and converge to an accurate position fix. Following initialisation, the RTK and standalone GPS solutions were implemented, and the data was logged to file. Both cases were tested for a period of 40 min, as it would allow for many samples while also exceeding the flight time of most quadcopters.

Additional steps were required for the RTK solution to ensure optimal performance. Firstly, the RTK solution is only possible if both the rover and base station maintain visibility with a minimum of five satellites. As a

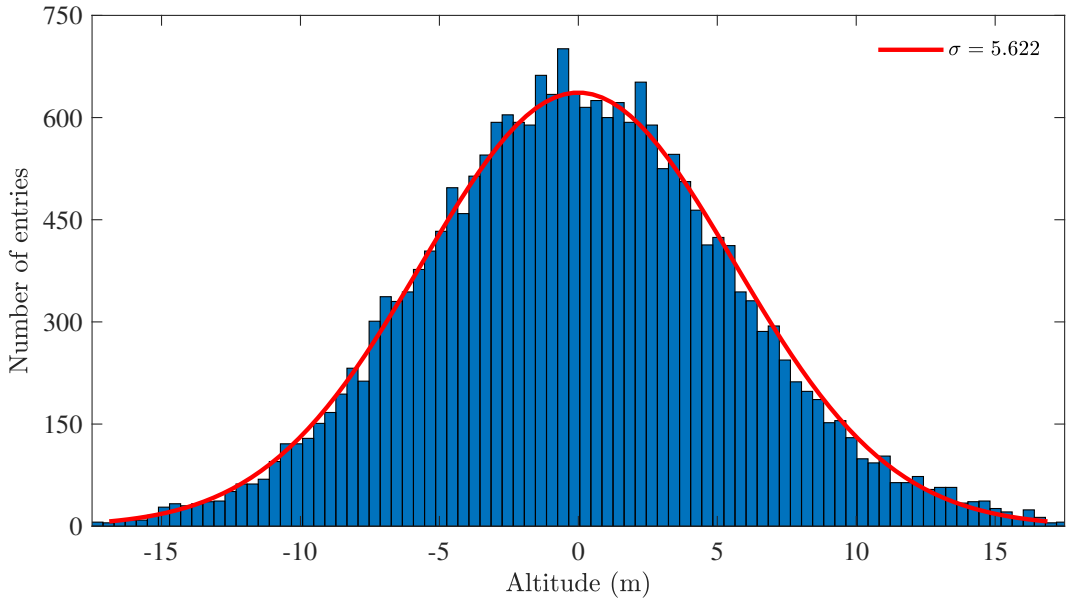

Figure A.1: Probability Distribution of the GPS Noise

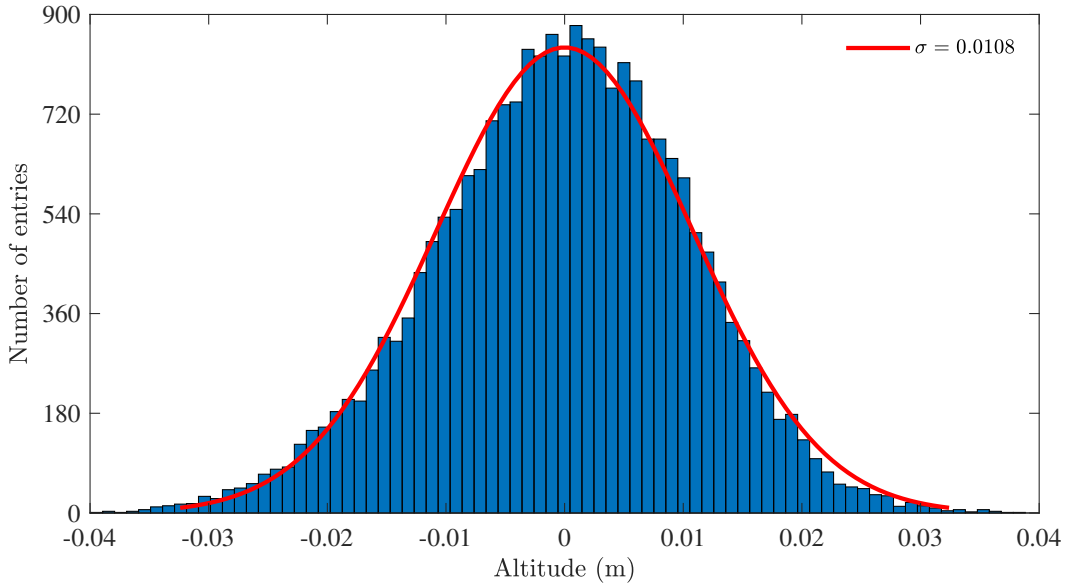

Figure A.2: Probability Distribution of the RTK-GPS Noise

verification, over the test period, the number of visible satellites varied between 7 and 8, thus ensuring optimal accuracy and data quality.

Secondly, the RTK solutions are provided as either a fixed or float solution, with the fixed solution being the more accurate of the two. Initially, the solution starts as a float solution and converges to the fixed solution with time, provided the signal is not obstructed. Once the solution converges to the fixed solution and then is obstructed, it reverts to the approximated float solution and restarts the convergence process.

Thus, for the collection of the RTK solution data, the logging process was started after the convergence to the fixed solution has completed. The tests were conducted twice over two different days to ensure accuracy, and the second set was used as verification for the calculated sensor noise. The collected data was analysed using MATLAB and the standard deviations for each of the sensors calculated. Additionally, the normal distributions for each of the two cases were also generated and are illustrated by Figures A.1 and A.2.

A.2 MEAS MS5611 Barometric Pressure Sensor

In the case of the barometer, the effect of the bias or barometer drift is unknown. Similar to the GPS and RTK-GPS cases, the barometer measurements are to be logged and analysed. As the barometer is integrated as part of the Pixhawk 1 flight controller, the Pixhawk was set up in a closed room to create a controlled environment. Using MAVLINK and QGroundControl, in addition to the PX4 flight stack, the Pixhawk was powered and the barometer altitude measurements were logged. Once again, similar to the Piksi, the tests lasted 40 min, the data logged to file and analysed using MATLAB.

As the collected barometer altitude measurements are in terms of pressure, the data is to be converted to a distance in meters. This was done using the barometric formula,

$$P = P_0 \cdot e^{\frac{-g \cdot M \cdot \Delta h}{R \cdot T}} \tag{A.1}$$

with the parameters, values and units summarized in Table A.1.

Using Equation A.1, the altitude was converted and plotted using MATLAB. For the identification of the barometer drift, a line of best fit was added to the data and illustrated in Figure A.3. Using the identified line of best fit, the barometer drift was modelled as a ramp function in Simulink. Thus, increasing at a constant rate based on the gradient of the fitted line, with the resulting signal added to the actual altitude of the drone.

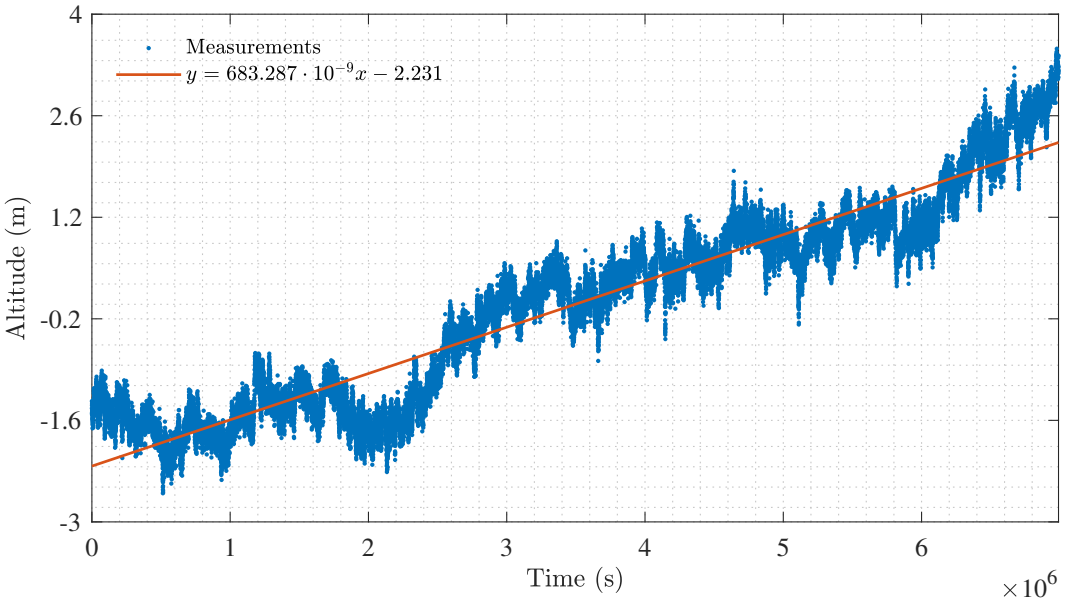

Figure A.3: Quantification of the Barometer Drift

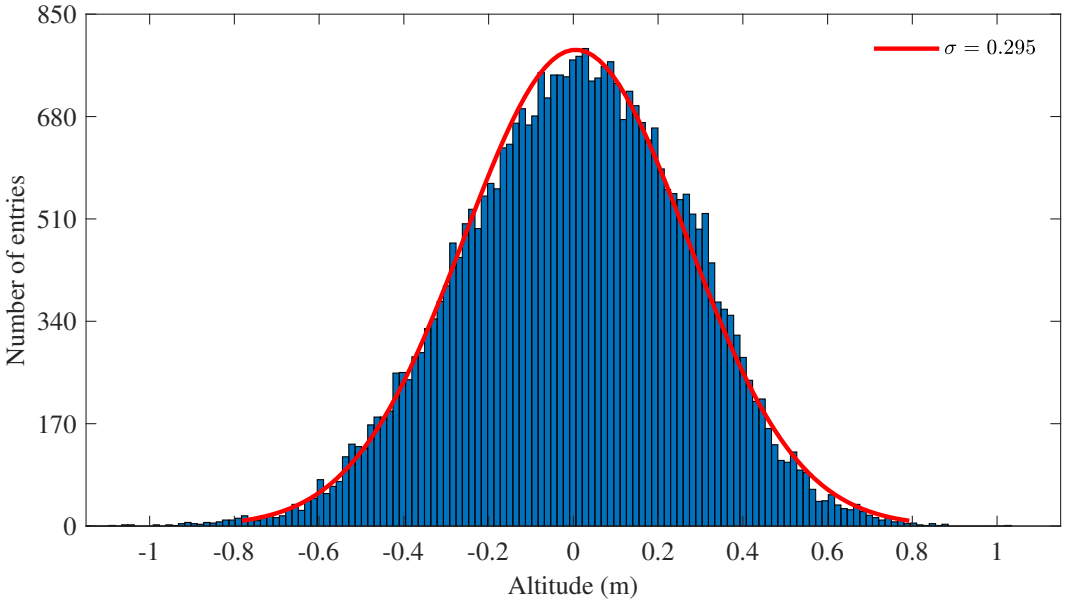

Figure A.4: Probability Distribution of the Barometer Noise

Table A.1: Barometric Formula Parameters

Parameter	Symbol	Value	Units
Altitude pressure	P	-	Pa
Reference pressure	P_0	-	Pa
Gravitational acceleration	g	9.810	$\mathrm{m\,s^{-2}}$
Molar mass of air	M	28.964×10^{-3}	$\mathrm{kg\,mol^{-1}}$
Difference in altitude	Δh	-	m
Reference temperature	T	-	K
Universal gas constant	R	8.314	$\mathrm{J\,mol^{-1}\,K}$

Furthermore, the barometer also exhibits noise in terms of a random error, similar to the Piksi and requires identification. Using the converted barometer altitude measurements, the probability distributions of the measurements were calculated, taking care to avoid inaccuracies due to the drift. This was done by normalizing the data using a centred moving average spanning an interval of 1 min. The normalised data was used and the normal distribution for the entire range determined as illustrated by Figure A.4. Additionally, similar to the Piksi tests, multiple data sets were collected and used to validate the parameters, with the final identified sensor noise parameters shown in Table 3.1.

List of References

Ajgl, J., Simandl, M. and Dunik, J. (2009). Millman's Formula in Data Fusion. In: *The 10th International PhD Workshop Young Generation Viewpoint*.
Available at: `https://www.researchgate.net/publication/216410994_Millman's_Formula_in_Data_Fusion`

Bancroft, J.B. and Lachapelle, G. (2011). Data fusion algorithms for multiple inertial measurement units. *Sensors*, vol. 11, no. 7, pp. 6771–6798. ISSN 14248220.

Bar-Shalom, Y. and Campo, L. (1986). The effect of the common process noise on the two-sensor fused-track covariance. *IEEE Transactions on Aerospace and Electronic Systems*, vol. AES-22, no. 6, pp. 803–805. ISSN 00189251.

Błachuta, M., Czyba, R., Janusz, W. and Szafrański, G. (2014). Data Fusion Algorithm for the Altitude and Vertical Speed Estimation of the VTOL Platform. *Journal of intelligent & robotic systems*, vol. 74, no. 1, pp. 413–420. ISSN 0921-0296.

Buczkowski, A. (2017). How accurate is your drone survey? everything you need to know.
Available at: `https://www.geoawesomeness.com/accurate-drone-survey-everything-need-know/`

Contreras, A.M. and Hajiyev, C. (2019). Robust Kalman filter-based fault-tolerant integrated baro-inertial-GPS altimeter. *Metrology and Measurement Systems*, vol. 26, no. 4, pp. 673–686.
Available at: `www.metrology.pg.gda.pl`

Dronecode (2019). PX4 Autopilot User Guide (master).
Available at: `https://docs.px4.io/master/en/`

DroneDeploy (2020). How accurate is my map?
Available at: `https://support.dronedeploy.com/docs/how-accurate-is-my-map-2`

Fong, L.-W. (2011). Multisensor measurement fusion via adaptive state estimator. In: *International Conference on Electric and Electronics*, vol. 100, pp. 455–462. Springer, Nanchang, China.
Available at: `https://www.researchgate.net/publication/241039942`

GPS.gov (2020). GPS.gov: GPS Performance.
Available at: `https://www.gps.gov/systems/gps/performance/`

Groves, P.D. (2013). *Principles of GNSS, Inertial, and Multisensor Integrated Navigation Systems*. Artech House, Norwood. ISBN 1608070050.

Hartman, D., Landis, K., Moreno, S. and Mehrer, M. (2014). Quad-Sim - File Exchange - MATLAB Central.
Available at: `https://www.mathworks.com/matlabcentral/fileexchange/48053-quad-sim`

Ho, P.-F., Hsu, C.-C., Chen, J.-C. and Zhang, T. (2018). Using Barometer on Smartphones to Improve GPS Navigation Altitude Accuracy. In: *Proceedings of the 24th Annual International Conference on mobile computing and networking*, MobiCom '18, pp. 741–743. ACM. ISBN 1450359035.

International Geosynthetics Society (2020). International Geosynthetics Society | IGS.
Available at: `https://www.geosyntheticssociety.org/`

InvenSense (2013). MPU-6000 and MPU-6050 Product Specification. Tech. Rep., InvenSense.
Available at: `https://invensense.tdk.com/wp-content/uploads/2015/02/MPU-6000-Datasheet1.pdf`

National Geospatial-Intelligence Agency (2020). Home | National Geospatial-Intelligence Agency.
Available at: `https://www.nga.mil/`

Renfro, B., Stein, M., Reed, E., Morales, J. and Villalba, E. (2019). An Analysis of Global Positioning System (GPS) Standard Positioning Service Performance for 2019. Tech. Rep., The University of Texas, Austin, Texas.
Available at: `https://www.gps.gov/systems/gps/performance/2019-GPS-SPS-performance-analysis.pdf`

Rice, J.A. (1995). *Mathematical Statistics and Data Analysis*. 2nd edn. Duxbury, Belmont, Calif. ISBN 0534209343.

Shin, V., Lee, Y. and Choi, T.S. (2006). Generalized Millman's formula and its application for estimation problems. *Signal Processing*, vol. 86, no. 2, pp. 257–266. ISSN 01651684.

Swift Navigation (2016). Piksi Datasheet. Tech. Rep., Swift Navigation.
Available at: `https://www.swiftnav.com/sites/default/files/piksi_datasheet_v2.3.1.pdf`

TE Connectivity (2017). MS5611-01BA03 Barometric Pressure Sensor. Tech. Rep., TE Connectivity.
Available at: `https://www.amsys-sensor.com/downloads/data/MS5611-01BA03-AMSYS-datasheet.pdf`

Torresol (2017). Gemasolar | Torresol Energy.
Available at: `https://torresolenergy.com/gemasolar/`

Wei, S., Dan, G. and Chen, H. (2016). Altitude data fusion utilising differential measurement and complementary filter. *IET Science, Measurement & Technology*, vol. 10, no. 8, pp. 874–879. ISSN 1751-8822.

Whang, I.-H. and Ra, W.-S. (2008). Simple altitude estimator using air-data and GPS measurements. In: *17th IFAC World Congress*, pp. 4060–4065. Seoul, Korea.

Zaliva, V. and Franchetti, F. (2014). Barometric and GPS altitude sensor fusion. In: *IEEE International Conference on Acoustic, Speech and Signal Processing (ICASSP)*, pp. 7575–7579. ISBN 9781479928934.

Zhang, L., Ma, Y., Liu, G. and Yu, Y. (2019). Multi-Sensor Fusion Quadrotor Attitude and Altitude Estimation. In: *Proceedings of the 2019 International Conference on robotics systems and vehicle technology*, RSVT '19, pp. 131–137. ACM. ISBN 9781450362429.